creative commons
COMMONS DEED

저작자표시-비영리-변경금지 2.0 대한민국

이용자는 아래의 조건을 따르는 경우에 한하여 자유롭게

- 이 저작물을 복제, 배포, 전송, 전시, 공연 및 방송할 수 있습니다.

다음과 같은 조건을 따라야 합니다:

저작자표시. 귀하는 원저작자를 표시하여야 합니다.

비영리. 귀하는 이 저작물을 영리 목적으로 이용할 수 없습니다.

변경금지. 귀하는 이 저작물을 개작, 변형 또는 가공할 수 없습니다.

- 귀하는, 이 저작물의 재이용이나 배포의 경우, 이 저작물에 적용된 이용허락조건을 명확하게 나타내어야 합니다.
- 저작권자로부터 별도의 허가를 받으면 이러한 조건들은 적용되지 않습니다.

저작권법에 따른 이용자의 권리는 위의 내용에 의하여 영향을 받지 않습니다.

이것은 이용허락규약(Legal Code)을 이해하기 쉽게 요약한 것입니다.

Disclaimer

dCollection

Ph.D. Dissertation of Biological Science

Studies on *de novo DSCAM* mutation from autism spectrum disorder patient using neurons induced from iPSC

유도 만능 줄기세포로부터 분화시킨 신경세포를 활용한 자폐아의 ***de novo DSCAM*** 돌연변이에 관한 연구

February 2023

Graduate School of Biological Science
Seoul National University
Brain Science Major

Min Jung Kim

Studies on *de novo DSCAM* mutation from autism spectrum disorder patient using neurons induced from iPSC

Advisor: Bong-Kiun Kaang

Submitting a Ph.D. Dissertation of
Seoul National University

December 2022

Graduate School of Biological Science
Seoul National University
Brain Science Major

Min Jung Kim

Confirming the Ph.D. Dissertation written by
Min Jung Kim
December 2022

Chair	이 용 석	**(Seal)**
Vice Chair	강 봉 균	**(Seal)**
Examiner	김 형	**(Seal)**
Examiner	임 채 석	**(Seal)**
Examiner	고 형 곤	**(Seal)**

ABSTRACT

Studies on *de novo DSCAM* mutation from autism spectrum disorder patient using neurons induced from iPSC

Min Jung Kim

School of Biological Science

The Graduate School

Seoul National University

Autism spectrum disorder (ASD) is one of the neurodevelopmental disorders characterized by difficulties with social interaction, and repetitive behaviors. The complexity of ASD pathology causes struggles with genetic remedies and patient-specific research. Recent advance in human induced pluripotent stem cell (iPSC) technique suggests an innovative methodology to design patient-specific-*in vitro* ASD model. Here, we generated induced neuronal (iN) cells from iPSC derived from an ASD patient with a heterozygous point mutation in the *DSCAM* gene. ASD iN cells show significantly decreased mRNA and protein levels of DSCAM compared to control iN cells. Then we figured out that genes related to trans-synaptic

signaling including NMDA receptor (R) subunits were down-regulated in ASD iN cells. NMDAR-mediated currents were also radically reduced in ASD iN cells. Defective NMDAR-mediated currents were restored by expressing wild-type DSCAM in ASD iN cells, whereas currents were significantly reduced by truncated DSCAM expression in control iN cells. Additionally, NMDAR subunit 1 (NR1) and DSCAM were co-localized in the neurites of iN cells, but co-localizations were significantly decreased in ASD iN cells. We suggest a low level of phospho-ERK1/2 in ASD iN cells as a potential mechanism with NMDAR function. These data suggest that heterozygous *DSCAM* mutation causes ASD pathology by NMDAR dysfunction.

Keyword: Autism spectrum disorder (ASD), DSCAM, NMDA receptor, induced pluripotent stem cell (iPSC), induced neuron (iN)

Student Number: *2020-35575*

CONTENTS

LIST OF FIGURES

CHAPTER I

INTRODUCTION

BACKGROUND

Neurodevelopmental disorders including autism spectrum disorder(ASD) show heterogeneous pathologies. The complexity of pathology confines individualistic research and generic therapies. The recent development of human-induced pluripotent stem cell (iPSC) technique suggests a new platform figure out complicated pathophysiological mechanisms of neurodevelopmental disorders. This study provides *in vitro* ASD model using iPSC technique and firstly suggests *DSCAM* mutation and ASD pathology.

Autism Spectrum Disorder

Autism Spectrum disorder (ASD) is one of the psychiatric disorders featured by constant difficulty with social interaction, repetitive behaviors, sensory abnormalities and intellectual disabilities in early manifestation in three-year-old or at least in childhood(Wilkins and Matson 2009, APA 2013, Grzadzinski, Huerta et al. 2013). Indeed, ASD is not rare disorder, as one of the 50 children is ASD patient (Srivastava and Schwartz 2014). Although ASD is relatively common disorder, it is considered as a severe mental problem. Based on the pathological treats, ASD patients are hard to be

harmonized in society. ASD is apparently diagnosed by the Diagnostic and Statistical Manual of Mental Disorders, Fifth edition (DSM-V) (APA 2013) (Figure 1), though status of the pathological severity is various among patients. Heterogeneous ASD pathologies makes hard to generate human *in vitro* model system and to study underlying molecular mechanisms.

According to the progress of gene discovery, tons of causative genes that induce ASD pathology, called ASD-associated genes, are unveiled (Srivastava and Schwartz 2014, Searles Quick, Wang et al. 2021). Specifically, genes related to regulation of other gene expressions, synaptic structure and function and chromatin remodeling are defected in ASD patients (Gilman, Iossifov et al. 2011, O'Roak, Vives et al. 2012, De Rubeis, He et al. 2014, Iossifov, O'roak et al. 2014). It is crucial to functionally categorize ASD-associated genes and to figure out their molecular pathways for the understanding of a series of ASD pathology and evaluating the potential pathogenic genes of ASD (Srivastava and Schwartz 2014).

DSM-V : Criteria of ASD
Social communication and social interaction
* Evidences of all following subdomains currently or previously. 1) Social reciprocity 2) Non-verbal communication 3) Developing, maintaining and understanding relationships
Restricted, repetitive behaviors and interests
* Evidences of 2 of 4 of following subdomains currently or previously. 1) Stereotyped, repetitive behaviors 2) Insistence on sameness 3) Highly restricted, fixed interests 4) Hypersensitivity or hyposensitivity in response to sensory inputs
Symptoms must be present in early development
Symptoms must cause clinically significant impairment in current functioning
Not better explained by intellectual disability or global developmental delay

Figure 1. DSM-V, Criteria of ASD

ASD diagnostic criteria, DSM-V, includes five symptom arrays (APA 2013).

Human induced pluripotent stem cell technology

Major hurdle of previous research of neuropsychiatric disorders are based on the transgenic mouse studies. Specific risk genes that have high possibility to trigger specific disorder are found through KO mouse model. However, research flow using transgenic mouse is hardly connected to the clinical studies, as these genes are not based patients' genetics. To overcome the challenge, recent studies use stem cells to generate patient-specific *in vitro* models (Wen, Christian et al. 2016). Through stem cell technique, induced cells with patient-specific genetic information can be generated.

Human iPSCs have been derived by using several methodologies such as virus, vectors, protein delivery, synthesized mRNA (Fusaki, Ban et al. 2009, Kim, Kim et al. 2009, Woltjen, Michael et al. 2009, Yu, Hu et al. 2009, Zhou and Freed 2009, Jia, Wilson et al. 2010, Warren, Manos et al. 2010). However, efficiency of reprogramming is relatively low in case of using established methods (Okita, Matsumura et al. 2011). Recent reprogramming is conducted by seven reprogramming factors with both suppressions of p53 and alteration of c-Myc into L-Myc (Okita, Matsumura et al. 2011).

Down syndrome cell adhesion molecule (DSCAM)

Down syndrome cell adhesion molecule (DSCAM) is one of the immunoglobulin (Zhang, Pak et al.) superfamily that contributes to the cell-to-cell interaction (Yamakawa, Huo et al. 1998). It is composed of a cytoplasmic domain, transmembrane (Schmucker, Clemens et al.) domain, 6 fibronectin (FN) domains with one Ig-like domain between FN4 and FN5, and 9 Ig-like domains in N-terminus. During the developmental stage, DSCAM contributes to the development of the nervous system including both central and peripheral ones through axonal guidance, dendritic patterning, and synaptic formation (Maynard and Stein 2012, Li, Sukeena et al. 2015).

DSCAM shows self-avoidance features that pushes away each other during neurite growth into axons or dendrites (Hattori, Millard et al. 2008). According to the previous studies of *Drosophila*, *Dscam* gene likely encodes above 30,000 various isomers (Schmucker, Clemens et al. 2000). Distinct isoforms could be formed by alternative exons including 12 types of Ig2 and 48 types of Ig3, 33 alternatives of Ig7, and 2 alternatives of TM (Wojtowicz, Flanagan et al. 2004). Recent studies show single neurons could express different isoforms, and various types of neurons could express a single set of isoforms (Neves, Zucker et al. 2004, Zhan, Clemens et al. 2004).

Through transgenic mouse studies, mice that are deleted exon 17 of *Dscam* showed shifted brain size, thinner cortical layers, and changed the

morphology of dendrites (Maynard and Stein 2012). These knock-out mice show reduced motor function and a deficit of motor learning (Li, Jiang et al. 2011). On the other hand, ASD patients show *DSCAM* variants, implying that *DSCAM* is one of the risk genes of ASD (De Rubeis, He et al. 2014, Iossifov, O'roak et al. 2014, Turner, Hormozdiari et al. 2016, Wang, Guo et al. 2016, C Yuen, Merico et al. 2017). However, it is veiled how cellular features of ASD in the human-based-neuronal model are triggered by *DSCAM* mutation.

N-Methyl-D-aspartate receptor (NMDA-R)

N-methyl-D-aspartate receptor (NMDA-R) is glutamate-mediated calcium channel and it is important to synaptic transmission (Paoletti, Bellone et al. 2013). There are different subtypes of NMDA-Rs according to the different subunit compositions (Cull-Candy and Leszkiewicz 2004, Traynelis, Wollmuth et al. 2010, Paoletti, Bellone et al. 2013). Based on the previous studies, there are 7 subunits, such as GluN1, GluN2A, 2B, 2C and 2D, GluN3A and 3B. In post-synaptic regions in mammalian brain, GluN1-GluN2A assembly and GluN1-GluN2A-GluN2B assembly exist dominantly, whereas assemblies including GluN2B are located in synaptic sites (Hardingham and Bading 2010, Gladding and Raymond 2011).

A composition of NMDA-R is dynamic in response to cellular activities by affecting synaptic function. During developmental stage,

subunit 2B is altered into subunit 2A in whole CNS (Dumas 2005). On the other hand, GluN3A expression that is peaked at postnatal state contributes to the maturation of NMDA-R (Henson, Roberts et al. 2010, Pachernegg, Strutz-Seebohm et al. 2012).

NMDA-R expression and function are crucial to ASD pathology (Lee, Choi et al. 2015). Clinical research show that ASD patient show genetic mutation of NMDA-R, specifically GluN2B (Tarabeux, Kebir et al. 2011, O'Roak, Vives et al. 2012, O'Roak, Vives et al. 2012, Kenny, Cormican et al. 2014).

PURPOSE OF THIS STUDY

Figuring out strong and effective treatments for neuropsychiatric disorders is important. Although tons of research regarding the molecular and cellular mechanisms of disorders (Pizzarelli and Cherubini 2011, Zhou and Parada 2012, Kenny, Cormican et al. 2014, Srivastava and Schwartz 2014, Gao and Penzes 2015, Rose, Niyazov et al. 2018), clear treatments have not been provided. The major reason why drug discovery is hard is that their pathological phenotypes are varied and heterogeneous (Chahrour, O'Roak et al. 2016). Due to complex traits, individualistic research using a patient-specific model is crucial. Patients could be categorized, if which individualistic triggering agent causes representative phenotypes of specific disorder. However, trials to generate in vitro patient-specific model have been rare. In this thesis, we present *de novo DSCAM* mutation in ASD patient and investigate pathological traits using *in vitro* model of ASD through the iPSC technique.

In chapter II, we start with the identification of *de novo DSCAM* mutation in ASD patient. *DSCAM* mutation is generated into induced neurons through the iPSC technique. We focus on whether in vitro disease model also shows decreased expression as well through molecular

experiments.

In chapter III, we conduct transcriptomic analysis to figure out up- or down-regulated genes in ASD iN cells. We specify NMDA-R components as functioning molecules among various down-regulated genes in ASD iN cells. Furthermore, the functionality of NMDA-R and the density of NR1 is measured through patch recording.

In chapter IV, to figure out whether mutated DSCAM affects NMDA-R expression and function, we expressed full-length DSCAM and mutated DSCAM in ASD iN cells and control iN cells respectively. Then NR1 density and NMDA-R-mediated currents were measured to verify DSCAM mutation effects on NMDA-R function. We also figure out the correlation between NMDA-R subunit 1 (NR1) and DSCAM. We conduct neurite analysis and proximity ligation assay (PLA) to unveil the expression of NR1 and the co-localization ratio between NR1 and DSCAM.

In this thesis, we discuss the correlation between patient-specific *DSCAM* mutation and ASD pathology using iPSC-derived induced neurons. Furthermore, we present rescuing pathological traits through normal DSCAM expression in ASD iN cells.

CHAPTER II

Identification of ASD patient-specific de novo mutation and generation of ASD iN cells

INTRODUCTION

Neuropsychiatric disorders including ASD show individualistic pathological traits and various triggering agents. Therefore, patient-specific research is required to make treatment of each pathology. Thanks to recent progress of stem cell technique, it makes possible to generate induced cells with patient's genetic information. In chapter II, we observe ASD patient-specific *de novo DSCAM* mutation through whole exome sequencing and generate *in vitro* disease model with patient's mutation by using iPSC technique.

At first, we figure out that there is no inheritance of ASD pathology through pedigree of ASD patient. Then, whole exome sequencing is conducted to four people in pedigree including ASD patient to find out genetic difference of patient from other family members. Observed ASD patient-specific mutation is generated with iPSCs and iN cells. In fact, previous research has presented forebrain regions including anterior cingulate cortex (ACC), medial prefrontal cortex (mPFC) are important to ASD pathology. We generate forebrain-like iN cells from iPSCs using Ngn2 method.

By using iN cells, we validate whether these neurons are real glutamatergic neurons and have patient-specific mutation. Then, we

quantify mRNA and protein level of DSCAM to figure out the relation between premature termination DSCAM mutation and DSCAM expression.

EXPERIMENTAL PROCEDURES

Patient description

A 12-year-old boy, was born at 39 weeks' gestation by spontaneous vaginal delivery with a birth weight of 3.5 kg after an uncomplicated pregnancy. He manifested autistic features before 36 months of age. His Autism Diagnostic Observation Schedule-2 (ADOS-2) testing demonstrated a total score of 15 (social affect score, 14; restricted and repetitive behavior score, 1) well within the range of an autism diagnosis at age five. His Autism Diagnostic Interview-Revised (ADIR) scores were also above the autism diagnostic cutoffs. In addition, he demonstrated severe sleep problems and a significantly high level of anxiety, with crying and screaming both at school and at home, particularly with his mother. He has intellectual disability and obesity at a weight of 79 kg and height of 165 cm. He has received early intervention since the age of 3 years old, but his behavior problems have continued throughout his childhood.

Whole exome sequencing

Whole blood was obtained from the patient and his family members (father, mother, and brother) after informed consent for the protocol (KNUH 2013-07-011-004) guided by the KNUH IRB. For each sample, approximately 27–31 million read pairs were generated. The generated raw sequencing reads were assessed and trimmed using the Sickle program (v. 1.33) to ensure the quality of the raw reads. Pre-processed reads were mapped to the reference human genome sequence GRCh37 using the Burrow-Wheeler Aligner (BWA, version 0.7.10) (Li, Handsaker et al. 2009). To reduce potential bias caused by the sequencing processes, the mapped duplicated reads were marked using Picard (v. 1.118). Insertion and deletion (INDEL) realignment and base quality recalibration were performed using GATK (version 3.2.2) (McKenna, Hanna et al. 2010). Using the alignments, small nucleotide variants (SNVs) and small INDELs were called by the GATK HaplotypeCaller, and called variants were filtered using the GATK variant quality score recalibration process. *De novo* variants were identified by Triodenovo (v. 0.04) (Wei, Zhan et al. 2015)and further filtered to exclude those included in dbSNP142, 1000 Genomes Project (Oct 2014), NHLBI-ESP project with 6500 exomes, or ExAC 65,000 exomes at the level of 1% minor allele frequency (MAF) by ANNOVAR (Wang, Li et al. 2010). In addition, the *de novo* variants were filtered out if they were present in the in-house genome and exome databases.

Generation of iPSCs

All experimental procedures for fibroblasts and iPSCs were approved by the Kyungpook National University Hospital IRB (KNUH 2013-07-011-004) and the Hannam University IRB (HANNAM 2013-12k). Patient-specific ASD iPSC lines (ASD#3, ASD#4, or ASD#5) were generated from skin fibroblasts of the 5-year-old boy (now 12-year-old) with ASD symptoms, and a sibling control iPSC line (Control#3) was generated from skin fibroblasts of his 3-year-old male sibling (now 10-year-old) without ASD symptoms using the integration-free method as previously described (Okita, Matsumura et al. 2011). Other control iPSC lines (Control#1 and Control#2) were also generated from skin fibroblasts of a 37-year-old healthy female or 8-year-old healthy boy, respectively. Cultured fibroblasts from skin biopsies were transfected with vectors containing OCT3/4, shp53 RNA, SOX2, L-MYC, or LIN28 via electroporation (Invitrogen, Neon^{TM} transfection system, MP922114). Seven days after transfection, fibroblasts were re-seeded onto a feeder layer of mouse embryonic fibroblasts (MEFs). The cells were maintained in an embryonic stem cell (ESC) medium containing 20% knockout serum, β-mercaptoethanol (Gibco, 21985023), 1x GlutaMAX (Gibco, 35050-061), 1x MEM-NEAA (Gibco, 11140050), penicillin/streptomycin (Hyclone, SV30010), and DMEM-F12 (Gibco, 11320-033). Three to four weeks after

iPSC induction, the iPSC-like colonies were picked and transferred onto new feeder layers. After passage 5, iPSC colonies were transferred into a feeder-free cell culture dish coated with vitronectin (Gibco, A14700) and maintained in Essential 8 media (Gibco, A1517001) supplemented with Essential 8 supplement and penicillin/streptomycin.

Neuronal induction from iPSCs

Induced neuronal (iN) cells were generated as described previously (Zhang, Pak et al. 2013), with minor modifications. First, culture plates were coated with Matrigel (Corning, 354230), iPSCs were dissociated with Accutase (Innovative Cell Technologies, AT104), and cells were plated at a density 80,000 cells/cm^2 in mTeSR1 medium (w/ supplement) (Stemcell Technologies, 85850) containing 10 μM Y-27632 (Tocris, 1254). The culture media was replaced the next day with fresh mTeSR1 (w/ supplement) containing rtTA+Ngn2 lentiviruses. On day 0, 2 mg/mL doxycycline (Sigma, D9891) was added to induce TetO gene expression after replacing the culture medium with DMEM/F12 medium (Gibco, 11320033) supplemented with 1% N2 (Gibco, 17502-048), 1% MEM nonessential amino acids (Gibco, 11140050), 10 ng/mL human BDNF (PeproTech; 450-02), 10 ng/mL human NT-3 (PeproTech; 450-02), and 0.2 μg/ml mouse laminin

(Sigma, L2020). On day 1, 1 μg/mL puromycin (Merck, 540411) was added to the culture for 24 hours to select virus-infected cells. On day 2, the culture medium was replaced again with a 1:1 mixture of glia-conditioned medium (GCM) and Neurobasal medium (Gibco, 21103-049) supplemented with B27 (Gibco, 17504-044) and Glutamax (Gibco, 35050-061). Additionally, 10 ng/mL BDNF, 10 ng/mL NT3, 2 mg/mL doxycycline, and 1 μg/mL puromycin were added to the culture. GCM was prepared by incubating mouse glial cells with Neurobasal medium supplemented with B27 and Glutamax for 24 hours. From day 4~8, 50% of the medium was replaced every other day. One to two μmol of cytosine-β-*d*-arabino-furanoside (Sigma, C-6645) was added to the cultures when other proliferating cell types were present. On day 9, neurons were dissociated with 0.25% Trypsin (Hyclone, SH30042.01) and plated at 30,000 cells/cm^2 on Matrigel-coated coverslips containing a monolayer of mouse glial cells in Neurobasal medium supplemented with B27, Glutamax, BDNF, NT3, doxycycline, and 2.5% fetal bovine serum (FBS, WelGENE, S001-01). Neurons were transfected with the indicated plasmids using Lipofectamine® 2000 reagent (Invitrogen, 11668-019) using the manufacturer's protocol.

Lentivirus generation

Lentiviruses for converting iPSC lines to induced neuronal (iN) cells were prepared according to a previous paper (Zhang, Pak et al. 2013),

with some modifications. In brief, Lenti-X 293T cells (Clontech, 632180) were co-transfected with Ngn2-expressing plasmid (13.3 μg), packaging plasmid (psPAX2, 10 μg), and VSV-G envelope plasmid (pMD2.G, 3.3 μg) using the calcium phosphate method. Six to eight hours after transfection, cultures were washed with DMEM and given fresh DMEM with 10% FBS, 2 mM L-Glutamine, and penicillin/streptomycin. Supernatant containing viruses was harvested 72 hours after transfection, centrifuged (20,000 rpm for 2 h), and filtered with a 0.22 μm syringe filter (Sartorius, 16534). Viral pellets were suspended with 200 μL of DMEM/F12 (Gibco, 11320-033). The viral titer was determined by measuring the GFP expression level after treatment with the viruses to Lenti-X 293T cells.

RESULTS

Genetics and clinical features of the ASD patient

We focused on the ASD patient who is a 12-year-old boy with early manifestation of ASD symptoms. Total score of Autism Treatment Evaluation Checklist (ATEC) is above 100, suggesting high severity among ASD patients (Figure 2A). In fact, 30^{th} percentile of ASD patients commonly get less than 50 in ATEC. ASD patient has had difficulties to adapt to school. His family depicted his pathological features, which consist of hyperactivity, lack of conversation, sleeping interruption, and over-eating. We conducted exome sequencing to patient's family members and figured out *DSCAM de novo* mutation only in patient (Figure 2B, C). Through Sanger sequencing technique, single mutation that found in *DSCAM* is unveiled as a base deletion in cDNA position 2051. This point mutation causes N-terminal truncated form of DSCAM by inducing early termination codon (L684X) between Ig 7 and Ig 8 (Figure 2D).

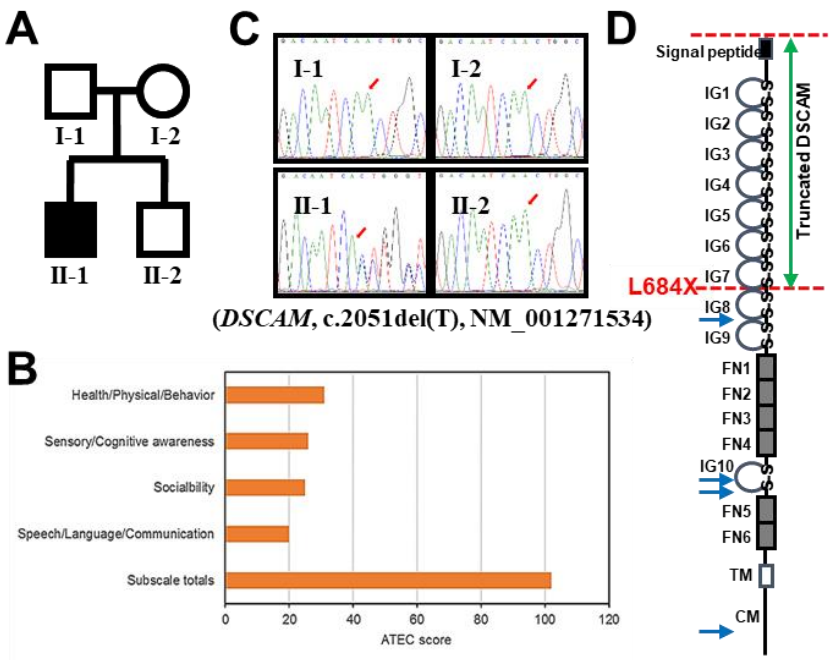

Figure 2. *De novo* single nucleotide deletion in the *DSCAM* gene of an ASD patient.

(A) Pedigree of the ASD family. The black filled symbol represents the ASD patient (II-1). (B) Autism Treatment Evaluation Checklist (ATEC) score of the ASD patient before intervention. (C) Whole exome sequencing was performed on four family members (I-1, I-2, II-1, and II-2). Confirmation of the identified single nucleotide deletion in the *DSCAM* gene. The single nucleotide deletion (*DSCAM*, c.2051del) identified in the ASD patient was validated by Sanger sequencing of the genomic DNA from four family members. The *DSCAM* transcript, NM_001271534 (RefSeq sequence) with the single nucleotide deletion (c.2051del; cDNA position 2051) is translated into a truncated form of the DSCAM protein due to an early stop codon at amino acid position 684, leucine (pL684X). (D) Schematic diagram of the

DSCAM protein with the termination site (L684X), which is located between the immunoglobulin (Zhang, Pak et al.) 7 and 8 domains of DSCAM. Other predicted truncation mutations reported previously (Satterstrom, Kosmicki et al. 2020) are indicated by blue arrows (IG: immunoglobulin domain; FN: fibronectin type III domain; TM: transmembrane domain; CM: cytoplasmic domain).

These experiments were performed in collaboration with Ji-Hye Kwak, Hyunhyo Seo, Kyungmin Lee.

Generation and depiction of ASD induced neuronal cells

To figure out pathological phenotypes of the N-terminal truncated DSCAM expression, control iPSC lines (control#1, #2, #3, #4) and ASD iPSC lines (ASD#3, #4, #5) were made by using fibroblasts of healthy people and ASD patient (Figure 3, 4). Stem cell colonies of control and ASD lines show common round-shaped morphology with packed form (Figure 5A). Then, we validated the pluripotency of iPSC lines by using alkaline phosphatase response, immunocytochemistry, and qPCR with stem cell markers (Nanog, Rex1, Sox2, and Oct3/4) (Figure 3).

To identify cellular phenotypes triggered by heterozygous *DSCAM* mutation, forebrain-like induced neuronal cells are generated from iPSCs through previously depicted methods (Zhang, Pak et al. 2013)(Figure 5). The neuronal differentiation rate is quantified by counting Ngn2-expressing cells and Tuj1-immunostained cells with glia co-culture. The differentiation rate shows no difference between control and ASD iN cells (Figure 5C). To identify the efficiency of the differentiation method through vGluT1-immunostaining with 2-week iN cells. Above 95 percent of iN cells are vGluT1-positive, indicating that the Ngn2 differentiation method can effectively induce glutamatergic iN cells from iPSCs, as previously described (Zhang, Pak et al. 2013). *DSCAM* mutation is conserved from fibroblast of ASD patient to ASD iPSCs and ASD iN cells by using genomic sequencing (Figure 6).

Then, we checked whether *DSCAM* mutation perhaps affects DSCAM expression in ASD iN cells. DSCAM expression is significantly reduced in ASD iN cells at the level of mRNA and protein (Figure 7).

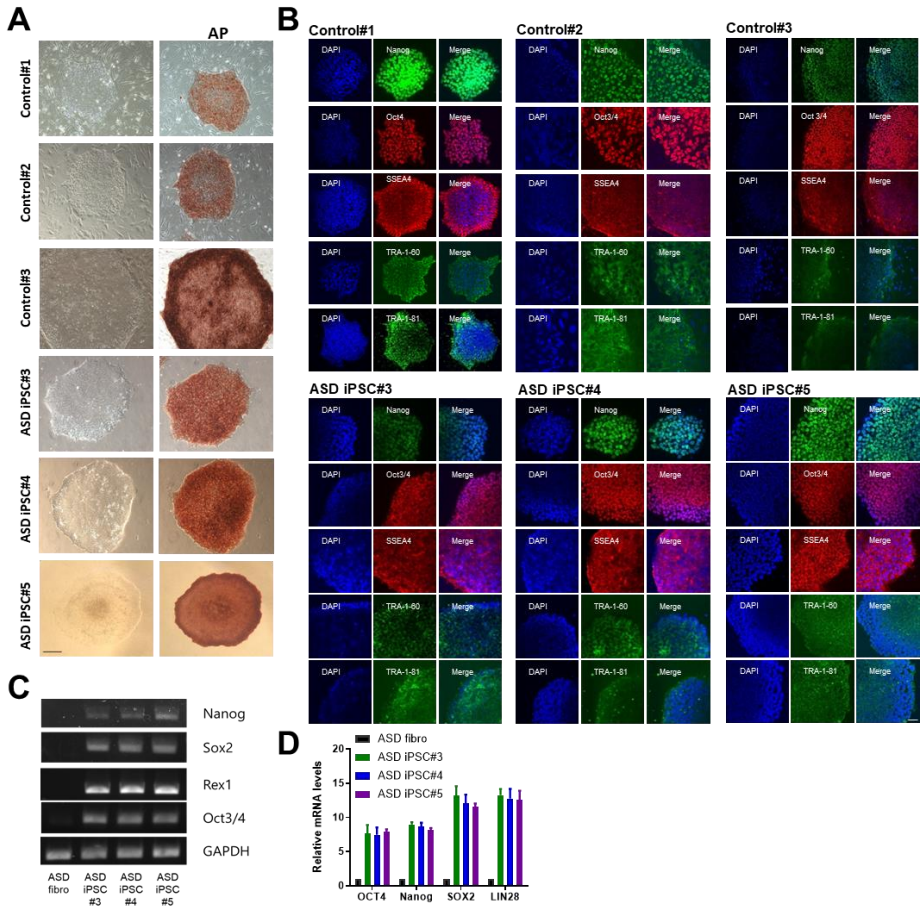

Figure 3. Characterization of human induced pluripotent stem cells (iPSCs) derived from fibroblasts.

(A) Morphology of iPSC colonies and alkaline phosphatase staining in iPSCs. Scale bar: 200 μm. (B) Immunostaining of human iPSCs with specific antibodies against intracellular pluripotent stem cell markers (Oct3/4, SSEA3, SSEA4, Tra1-60, and Tra1-81). Scale bar: 50 μm. (C-D) qPCR analysis of pluripotency marker expression (Oct3/4, Sox2, Rex1, and Nanog) in iPSCs. Data in the bar graph are presented as the mean ± SEM.

These experiments were performed in collaboration with You-Kyung Lee and Jin-A Lee.

Line	Gender	Age	Origin	Disease	Reprogramming methodology	Ethnicity
Control #1	Female	37	Fibroblast	Normal	Episomal iPSC reprogramming plasmids / Electroporation	Asian
Control #2	Male	5	Foreskin	Normal	Episomal iPSC reprogramming plasmids / Electroporation	Asian
Control #3	Male	8	Fibroblast	Normal	Episomal iPSC reprogramming plasmids / Electroporation	Asian
Control #4	Male	Newborn	Fibroblast	Normal	Episomal iPSC reprogramming plasmids / Electroporation	-
ASD #3,4,5	Male	12	Fibroblast	ASD	Episomal iPSC reprogramming plasmids / Electroporation	Asian

Figure 4. List of iPSC lines used (Jung, Lee et al. 2018)

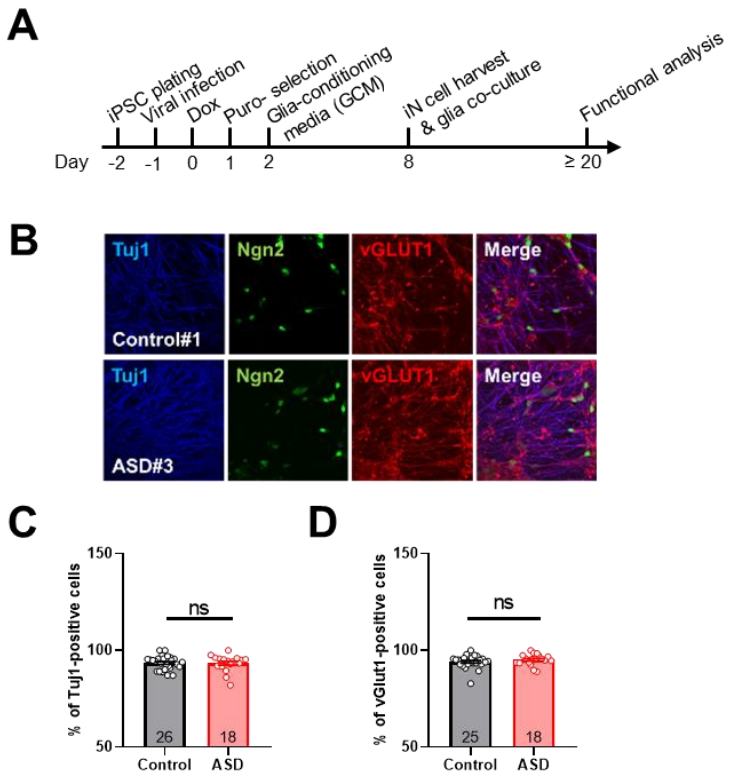

Figure 5. Generation of ASD iN cells from ASD iPSCs.

(A) Timetable of the differentiation procedure of iN cells from iPSCs. (B-D) Analysis of the differentiation of iPSCs to iN cells using Tuj1 (early neuronal marker) and vGlut1 (glutamatergic neuronal marker) antibodies revealed no difference between ASD and control iN cells. The number in the bars represents the independent culture number. (Kruskal–Wallis test for upper and lower left panels, ns, not significant, unpaired t-test for upper right panel, ns, not significant, Mann–Whitney test for lower right panel, ns, not significant). Scale bar: 50 μm.

These experiments were performed in collaboration with You-Kyung Lee and Jin-A Lee.

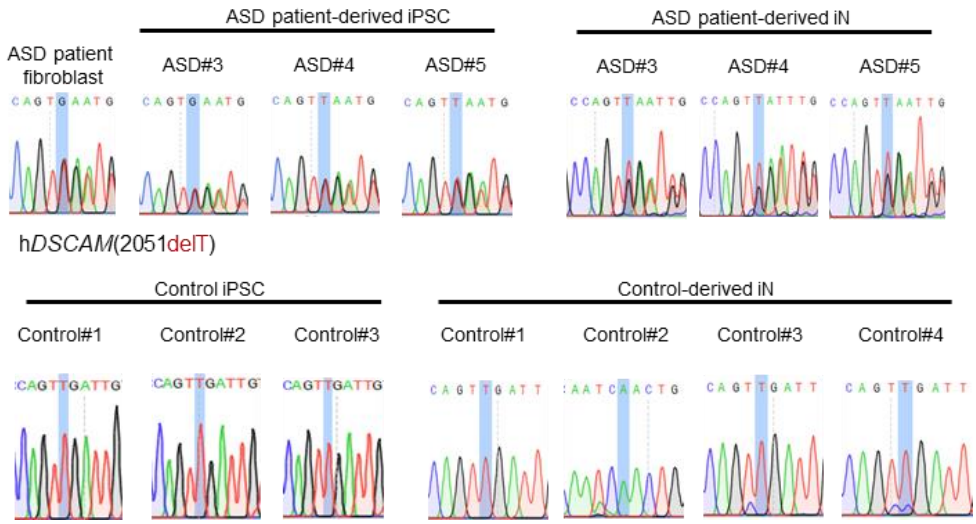

Figure 6. Genomic sequence of the DSCAM gene deletion mutation (2051del(T)) in fibroblasts and iPSC-derived neurons.

Genomic sequence of the *DSCAM* gene in ASD fibroblasts (or control fibroblasts) and iPSC-derived neurons showing the 2051del(T).

These experiments were performed in collaboration with Jung-eun Yang and Ro Un Lee.

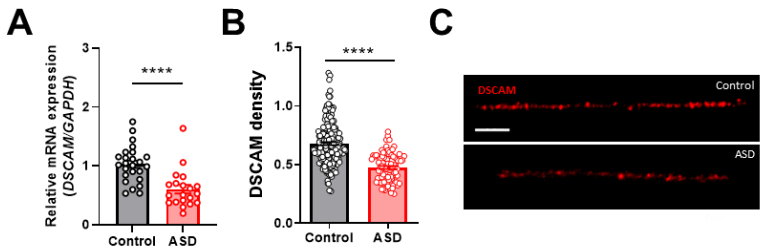

Figure 7. Characterization of ASD iN cells.

(A) DSCAM mRNA levels were significantly decreased in ASD iN cells [Control: n = 27, ASD: n = 20 (Control#1: n = 11, Control#2: n = 8, Control#3: n = 4, Control#4: n = 4, ASD#3: n = 10, ASD#4: n = 4, ASD#5: n = 6), Kruskal–Wallis test for left panel ($p < 0.01$), followed by Dunn's multiple comparisons test (Control#4 vs. ASD#3, *$p < 0.05$, Control#4 vs. ASD#4, *$p < 0.05$), unpaired t-test for right panel (****$p < 0.0001$)]. (B, C) Analysis of DSCAM expression in iN cells. DSCAM expression (the number of red signals) in the neurites (C) was significantly reduced in ASD iN cells as compared to control iN cells. (B) [one-way ANOVA for left panel (interaction, $p < 0.0001$, $F(6, 227) = 16.47$) followed by Tukey's multiple comparisons test (Control#1 vs. ASD#3, ***$p < 0.001$, Control#1 vs. ASD#4, ****$p < 0.0001$, Control#1 vs. ASD#5, ****$p < 0.0001$, Control#2 vs. ASD#3, **$p < 0.01$, Control#2 vs. ASD#4, ****$p < 0.0001$, Control#2 vs. ASD#5, ****$p < 0.0001$, Control#3 vs. ASD#4, **$p < 0.01$, Control#3 vs. ASD#5, ****$p < 0.0001$, Control#4 vs. ASD#3, *$p < 0.05$, Control#4 vs. ASD#4, ****$p < 0.0001$, Control#4 vs. ASD#5, ****$p < 0.0001$), Mann–Whitney test for right panel, ****$p < 0.0001$]. Scale bar: 100 μm.

DISCUSSION

In chapter II, ASD patient-specific *DSCAM* mutation is identified and generated into induced neurons. *DSCAM* is one of the significant ASD genes based on the genetic research of ASD (Satterstrom, Kosmicki et al. 2020).

In the case of humans, DSCAM is commonly expressed at the fetal developmental stage specifically in the brain. DSCAM mRNA is mainly observed in neurons and oligodendrocytes in the mammalian brain (Skene, Bryois et al. 2018). However, the relation between DSCAM mutation and ASD pathologies is still unknown. Furthermore, how DSCAM regulates NMDA-R function is veiled. In this chapter, we generate forebrain-like induced neuronal (iN) cells with *DSCAM* mutation from stem cells of ASD patients.

First, we generate iPSCs from the fibroblast of ASD patient, and iN cells are differentiated from iPSCs through the Ngn2 method. After the generation of *in vitro* disease model, the conservation of *DSCAM* mutation, 2051delT, is validated through genomic sequencing of each iPSCs and iNs. Interestingly, ASD lines with heterozygous mutated DSCAM show decreased expression of DSCAM in the level of mRNA and protein

compared to the control iN cells, suggesting genetic mutation of *DSCAM* perhaps regulates DSCAM expression.

CHAPTER III

DSCAM mutation causes decreased expression and dysfunction of NMDA-R

INTRODUCTION

In the previous chapter, we generate *in vitro* ASD model with heterozygous *DSCAM* mutation and find out decreased DSCAM expression in the level of mRNA and protein. The next step is to discover how *DSCAM* mutation causes ASD pathology. we speculate DSCAM mutation affects the expression of synaptic genes most of which are risk genes of ASD (He, Sanders et al. 2013, Egger, Roetzer et al. 2014, Cotney, Muhle et al. 2015). To test this hypothesis, we use RNA sequencing and specify gene groups that are downregulated in ASD iN cells.

In chapter III, we examine differentially expressed genes (DEG) in control and ASD iN cells respectively through transcriptomic analysis. After specifying genes that are significantly downregulated in ASD iN cells, we validate real mRNA expression through quantitative RT-PCR. Finally, we use immunocytochemistry and patch recording to figure out alterations in the expression and functionality of specified genes. In summary, chapter III data imply that *DSCAM* mutation decreases the expression of synaptic genes and triggers the dysfunction of a specific molecule.

EXPERIMENTAL PROCEDURES

RNA sequencing analysis

Total RNA was extracted from the iPSC-derived control and ASD iN cells. The quality and integrity of the extracted total RNA were assessed using BioAnalyzer and the standard Illumina sequencing system protocol (TruSeq RNA sample preparation kit v2) was used to make libraries for RNA sequencing. About 300-bp-long fragments were isolated using gel electrophoresis; they were then amplified by PCR and sequenced on Illumina HiSeq X platform in the paired-end sequencing mode (2 × 150 bp reads). Bioinformatics analysis were performed as described previously (Lee, Hwang et al. 2020). Briefly, raw sequencing reads were aligned to the human genome and differential gene expression analysis was conducted using the DESeq2 method (Anders and Huber 2010) and genes with at least 1.5-fold changes between groups at a false discovery rate (FDR) of 5% were defined as differentially expressed genes. The Metascape tool (Zhou, Zhou et al. 2019) was used for functional annotations for the differentially expressed genes identified.

Quantitative real-time PCR

To analyze the gene expression of each iPSC clone, total mRNA was extracted using Trizol (MRC, TR118) or the Monarch Total RNA Miniprep Kit (T2010S), and cDNA was synthesized using a Superscript III reverse transcription kit (Invitrogen, 18018-093; according to the manufacturer's instructions) or Luna Script RT Super Mix kit (E3010L). Real-time PCR was conducted using Taqman probes (Sox2 (Thermo, Hs00602736_s1), Nanog (Thermo, Hs02387400_g1), or Oct3/4 (Thermo, Hs00742896_s1)) with a Luna Script RT Super Mix kit (Applied Biosystems).

To analyze gene expression changes in the iN cells, quantitative RT-PCR was conducted with mRNAs extracted from 2-week-old iN cell cultures. RNA purification was performed with a Takara MiniBEST universal RNA extraction kit (Takara, #9767A) and cDNA was synthesized using a PrimeScript™ 1st strand cDNA Synthesis kit (Takara, #6110A). PCR was performed using specific primers presented in the Figure 12.

Immunocytochemistry

To examine the expression of stem cell markers in each iPSC clone, fixed cells were permeabilized with 0.1% Triton X-100 and blocked with 3% BSA. Primary antibodies (Oct3/4 (Santa Cruz, sc-5279), Nanog (Reprocell, RCAB003P-F), SSEA4 (abcam, ab16287), TRA-1-60 (Millipore,

MAB4360), and TRA-1-81 (Millipore, MAB4381) were incubated at 4℃ overnight, followed by incubation with secondary antibodies (Alexa Fluor 488 or Cy3-conjugated antibody) at RT for 1.5 h. Cell images were taken by a confocal microscope (Zeiss, LSM-880). For iN cells, 2-week- or 6-week-old iN cells were fixed by serial incubation with 4% paraformaldehyde and methanol (Moon, Cho et al. 2007). Fixed cells were blocked (5% normal goat serum, 0.05% Triton X-100 in PBS, pH 7.4), and then treated with primary antibodies MAP2 (Millipore, ab5622), phosphor-ERK1/2 (Cell Signaling, 9109), NR1 (BD Biosciences, 556308 or Synaptic Systems, 114011), DSCAM (LSBio, B5787), and tubulin (Sigma, T4026) followed by Alexa Fluor-conjugated secondary antibodies (Invitrogen). Three-dimensional (3D) reconstruction of neurites and quantification of immunostained puncta were performed using IMARIS (Bitplane, Zurich, Switzerland) software. Experimenters were blinded to the immunocytochemical samples until completing quantitative analyses.

Electrophysiology

Whole cell patch clamp recordings from iN cells were performed as previously described (Zhang, Pak et al. 2013) at room temperature while perfusing with a bath solution containing 140 mM NaCl, 5 mM KCl, 10 mM HEPES, 2 mM $CaCl_2$, 2 mM $MgCl_2$, and 10 mM glucose at pH 7.4. Membrane excitability was recorded at a membrane potential of -70 mV in

current clamp mode, during which stepwise currents were injected for 500 ms to elicit action potentials; current steps ranging from 0–60 pA were delivered at 10-pA increments. The pipette solution used for these recordings contained 145 mM K-gluconate, 5 mM NaCl, 10 mM HEPES, 1 mM $MgCl_2$, 0.2 mM EGTA, 2 mM MgATP, and 0.1 mM Na_3GTP (280 ~ 300 mOsm, adjusted to pH 7.2 with KOH). Miniature excitatory postsynaptic currents (mEPSCs) were recorded in voltage-clamp mode in the presence of picrotoxin (100 μM) and tetrodotoxin (1 μM). The internal solution used for recording contained 100 mM Cs-gluconate, 5 mM NaCl, 10 mM HEPES, 10 mM EGTA, 20 mM TEA-Cl, 3 mM QX-314, 4 mM MgATP, and 0.3 mM Na_3GTP (280~300 mOsm, pH adjusted to 7.2 with CsOH). Only cells with a <25% change in access resistance were included in the analysis with MiniAnalysis program (Synaptosoft). NMDA currents (I_{NMDA}) isolated with picrotoxin (100 μM) and CNQX (20 μM) were recorded in voltage-clamp mode in a bath containing 140 mM NaCl, 5 mM KCl, 10 mM HEPES, 2 mM $CaCl_2$, 0.8 mM $MgCl_2$, and 10 mM glucose (pH 7.4). NMDA-R-mediated currents were evoked by puff application (5 psi) of 100 μM NMDA and 10 μM glycine using 3–5 MΩ glass pipettes. Experimenters were always blinded to cell identities.

RESULTS

RNA sequencing analysis

To figure out the molecular mechanisms of heterozygous *DSCAM* mutation, transcriptomic features of control iN cells and those of ASD iN cells are compared through RNA sequencing. 877 upregulated genes and 928 downregulated genes are differentially identified (Figure 8A). Further, the investigation of molecular signatures of differentially expressed genes has experimented with through functional annotations analysis which is commonly used to figure out molecular pathways and genetic ontology. Specifically, downregulated genes in ASD iN cells are highly linked to “trans-synaptic signaling”, “axon development” and “synapse organization” (Figure 8B, left panel). Whereas, upregulated genes in ASD iN cells are related to the “extracellular matrix organization” and “elastic fiber formation” (Figure 8B, right panel). Intriguingly, the mRNA expressions of NMDA-R subunits, NR1, NR2B, and NR3A are radically decreased in ASD iN cells.

RNA sequencing analysis is approved with quantitative RT-PCR. Among various synaptic genes, NMDA-R subunits, *NR1*, and *NR2B*, are significantly reduced in ASD iN cells (Figure 9B, upper panel). Particularly,

NR1 expression was much more decreased compared to that of *NR2B*. On the other hand, expressions of *LRRTM1* and *SYT6*, genes contributing to synaptic signaling, are also reduced in ASD iN cells (Figure 9B, bottom panel). We also confirm whether ASD iN cells and control iN cells show different neuronal growth. However, dendritic growth shows no changes between control iN cells and ASD iN cells through Dendritic Sholl analysis (Figure 11).

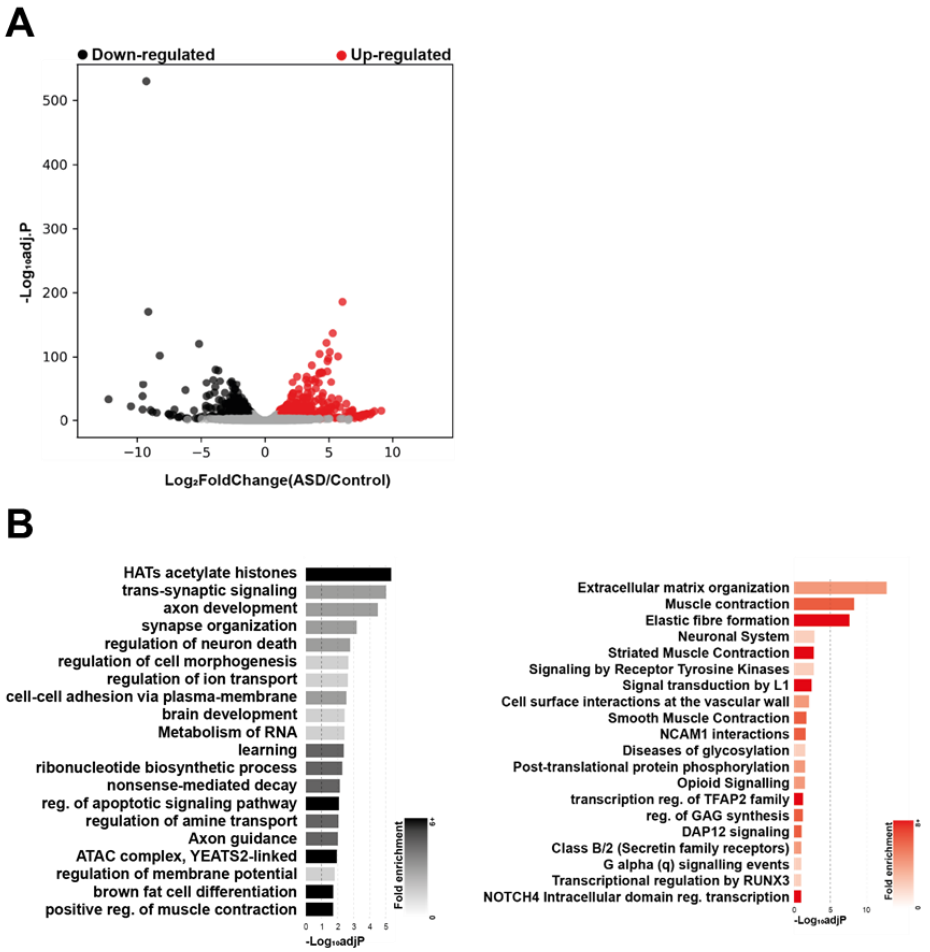

Figure 8. Transcriptomic analysis of ASD iN cells

(A) A volcano plot for differentially expressed genes between ASD and control iN cells. Significantly up-regulated genes are represented by red dots and black dots indicate significantly down-regulated genes in ASD iN cells. The X-axis is the log2-transformed gene expression in ASD iN cells divided by that in control cells. The Y-axis represents the *p*-value (−log10) adjusted by the multiple testing correction. (B) Gene ontology term and functional pathway enrichments in up-regulated (red) genes and down-regulated (black) genes in ASD iN cells by Metascape. The adjusted *p*-values of

significantly enriched terms or pathways are shown as bar plots.

These experiments were performed in collaboration with Kyu-Won Shim and Jae-Hyung Lee.

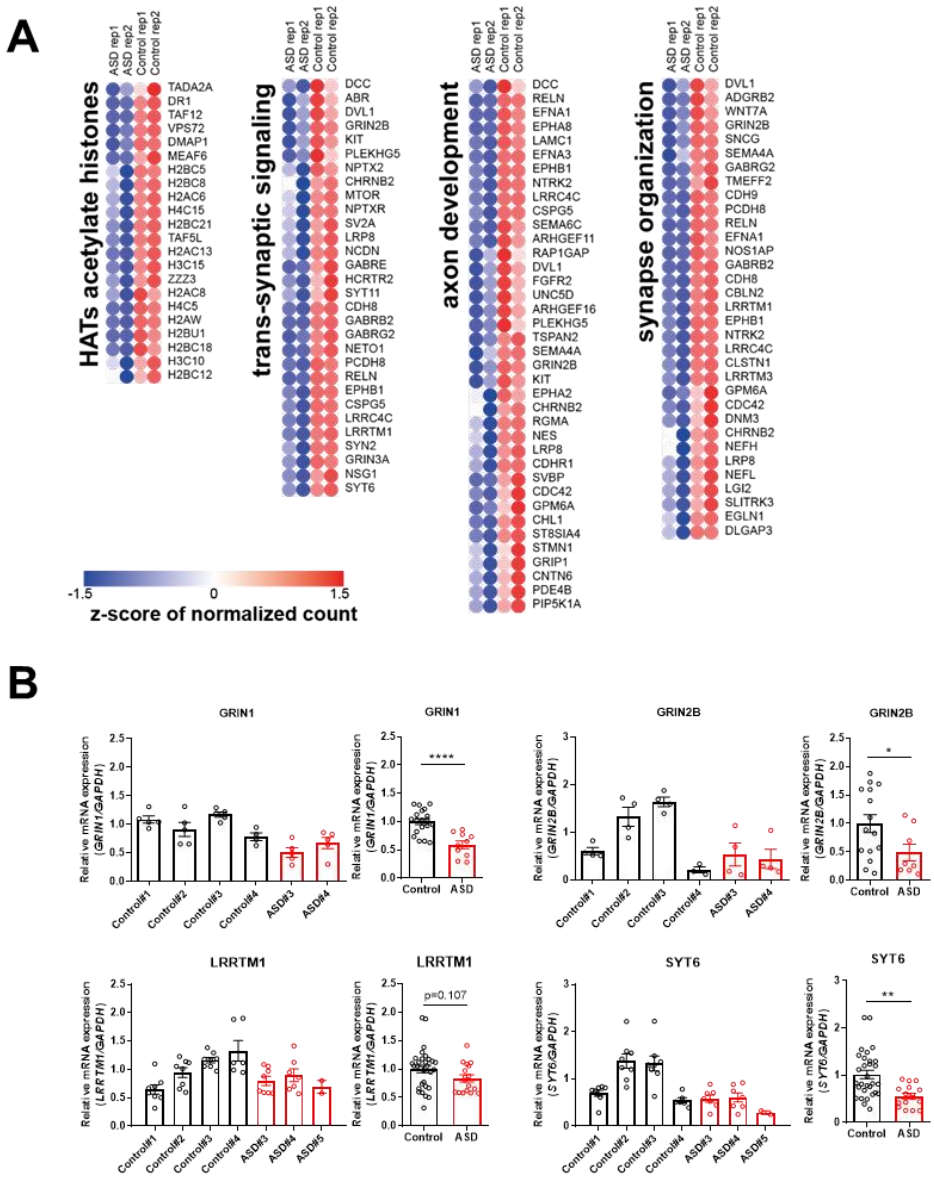

Figure 9. Categorization and validation of ASD downregulated genes

(A) Representative heat maps for the top four enriched terms or pathways (HATs acetylate histones, trans-synaptic signaling, axon development, and synapse organization) for the down down-regulated genes in ASD iN cells. (B) Quantitative RT-PCR analyses of mRNA expression level of *NR1*, *NR2B*, *LRRTM1*, and *SYT6* in 3-week-old iN cells. Each gene expression was

normalized to GAPDH expression. The NMDA-R components, *NR1* and *NR2B*, are decreased in ASD iN cells. For NR1 [Control: n = 19, ASD: n = 10 (Control#1: n = 5, Control#2: n = 5, Control#3: n = 5, Control#4: n = 4, ASD#3: n = 5, ASD#4: n = 5), unpaired *t*-test for right panels (****$p < 0.0001$)]. For NR2B [Control: n = 15, ASD: n = 8 (control#1: n = 4, control#2: n = 4, control#3: n = 4, control#4: n = 3, ASD#3: n = 4, ASD#4: n = 4), unpaired t-test for right panel, *$p < 0.05$]. For LRRTM1 [Control: n = 30, ASD: n =17 (Control#1: n = 8, Control#2: n = 8, Control#3: n = 8, Control#4: n = 6, ASD#3: n = 8, ASD#4: n = 7, ASD#5: n = 2), unpaired *t*-test for right panels, not significant ($p = 0.107$)]. For SYT6 [Control: n =30, ASD: n = 16 (Control#1: n = 8, Control#2: n = 8, Control#3: n = 8, Control#4: n = 6, ASD#3: n = 7, ASD#4: n = 7, ASD#5: n = 2), unpaired *t*-test for right panel (**$p < 0.01$)].

These experiments were performed in collaboration with Kyu-Won Shim and Jae-Hyung Lee.

Gene Name	Forward (5'→3')	Reverse (3'→5')
hDscam	TTGCGGTCTTCAAGTGCATTA	TGCAGCGGTAGTTATACAATCCA
GRIN1	ACCCCAAGATCGTCAACATTG	GGCTAACTAGGATGGCGTAGA
LRRTM1	TCGGGCAACGAGATCGAGTA	GCTTGTCAGGGACTTCCAAGA
SYT6	CTCCCGCCATGACATGATTG	TCCCAAGTCCACGCTTTCAC
Sox2	GGGAAATGGGAGGGGTGCAAAAGAGG	TTGCGTGAGTGTGGATGGGATTGGTG
Nanog	AAGACAAGGTCCCGGTCAAG	CAGGCATCCCTGGTGGTAG
Rex1	AAGGCAAGTCAAGCCAAGACC	TTCCAAAGAACATTCAAGGGAGC
Oct3/4	CCCCAGGGCCCCATTTTGGTACC	ACCTCAGTTTGAATGCATGGGAGAGC

Figure 10. Primer sequences for qRT-PCR

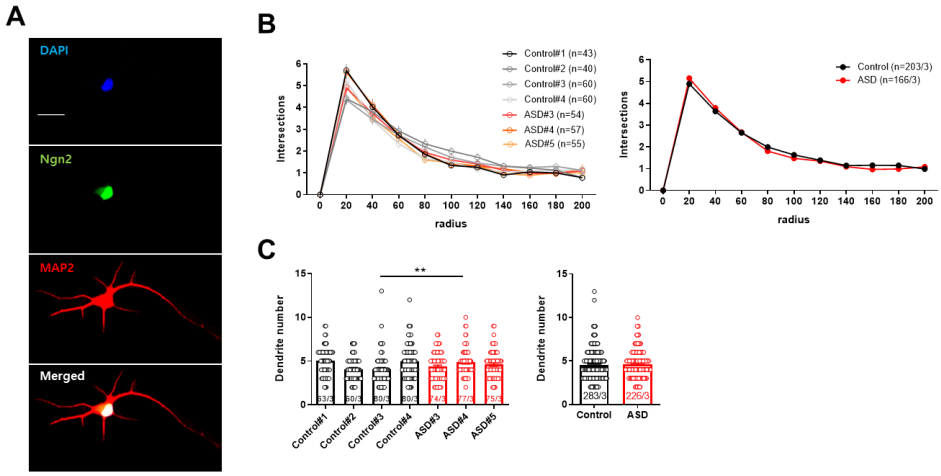

Figure 11. Dendritic analysis of iN cells

(A) Representative images of MAP2 staining. Scale bar: 30 um. (B) Dendritic Sholl analysis showed no difference between control and ASD iN cells [Control: n = 326, ASD: n = 226 (Control#1: n = 63, Control#2: n = 60, Control#3: n = 80, Control#4: n = 80, ASD#3: n =74, ASD#4: n = 77, ASD#5: n = 75); two-way repeated-measures ANOVA, interaction, F (10, 4781) = 1.756, p = 0.0632]. (C) The number of dendrites were comparable between control and ASD iN cells [Control: n = 283, ASD: n = 226 (Control#1: n = 63, Control#2: n = 60, Control#3: n = 80, Control#4: n = 80, ASD#3: n = 74, ASD#4: n = 77, ASD#5: n = 75), Kruskal-Wallis test for left panel ($p < 0.0001$, Control#1 vs Control#2, $*p < 0.05$, Control#1 vs Control#3, $***p < 0.001$, Control#3 vs Control#4, $**p < 0.01$, Control#3 vs ASD#4, $**p < 0.01$), Mann-Whitney test for right panel, p = 0.3512)].

These experiments were performed in collaboration with Ja Eun Choi.

NMDA-R-mediated currents are compromised in ASD iN cells

Transcriptomic analyses suggest decreased NMDA-R expression which has caused ASD pathologies. We test whether NMDA-R-mediated currents are changed according to the experimental groups through patch recording. The amplitude of NMDA-R-mediated currents is radically reduced in ASD iN cells (Figure 12). As among NMDA-R subunits, NR1, NR2A, and NR2B, *NR1* mRNA expression shows the notable decrease in ASD iN cells compared to the other subunits' expressions, further experiments are focused on the NR1 (Figure 13A). We also observed decreased NR1 protein level through immunocytochemistry (Figure 13B, C) in ASD iN cells.

Then, we check the electrophysiological features of ASD and control iN cells. There is no significant difference in resting membrane potential between ASD iN cells and control iN cells at -45mV with glial co-culture for 2 weeks (Figure 14A). Furthermore, membrane capacitance is similar in both control and ASD iN cells (Figure 14B). We observed large amplitude and reduced half-width of action potential in ASD iN cells (Figure 14C, D).

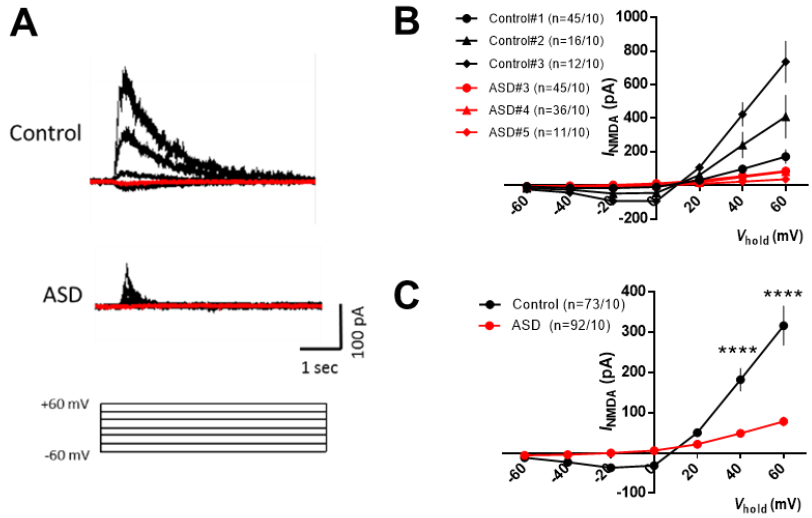

Figure 12. Compromised NMDA-R-mediated currents in ASD iN cells

(A-C) Voltage dependency of NMDA-R-mediated currents in control and ASD iN cells. Note the significantly lower NMDA-R-mediated currents at +40 and +60 mV in ASD iN cells (Control: n = 73, ASD: n = 92 from ten independent cultures; two-way repeated-measures ANOVA, interaction, F (6, 228) = 6.200, $p < 0.0001$; Bonferroni post hoc test, +40 mV, ****$p < 0.0001$; +60 mV, ****$p < 0.0001$)

These experiments were performed in collaboration with Ja Eun Choi.

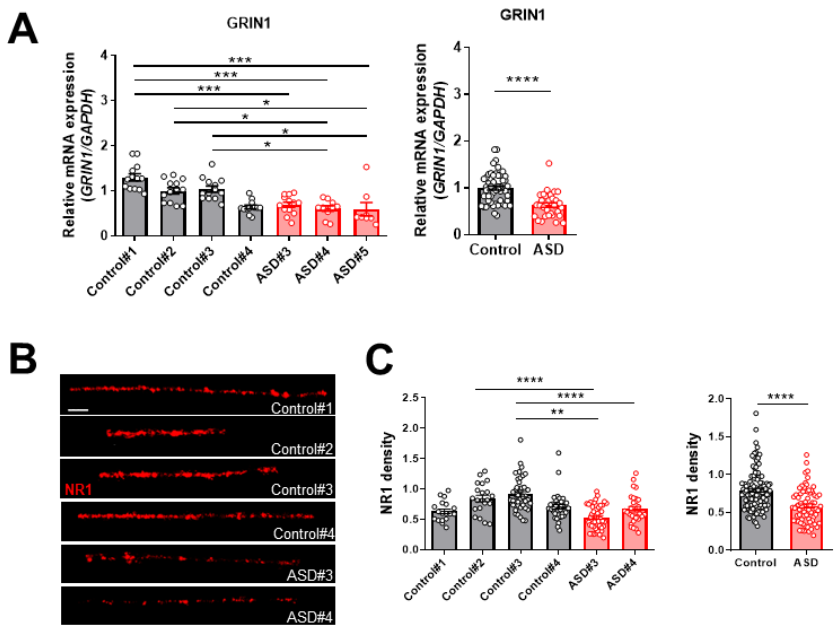

Figure 13. Decreased mRNA and protein expression of NR1

(A) Quantitative RT-PCR analysis of normalized *NR1* gene expression in control and ASD iN cells. The expression of *NR1* was significantly reduced in ASD iN cells. For *NR1* [Control: n = 51, ASD: n = 31 (Control#1: n = 13, Control#2: n = 13, Control#3: n = 13, Control#4: n = 12, ASD#3: n = 13, ASD#4: n = 10, ASD#5: n = 8), Kruskal–Wallis test for left panels ($p < 0.0001$) followed by Dunn's multiple comparisons test (Control#1 vs. Control#4, ****$p < 0.0001$, Control#1 vs. ASD#3, ***$p < 0.001$, Control#1 vs. ASD#4, ***$p < 0.001$, Control#1 vs. ASD#5, ***$p < 0.001$, Control#2 vs. Control#4, *$p < 0.05$, Control#2 vs. ASD#4, *$p < 0.05$, Control#2 vs. ASD#5, *$p < 0.05$, Control#3 vs. Control#4, *$p < 0.05$, Control#3 vs. ASD#4, *$p < 0.05$, Control#3 vs. ASD#5, *$p < 0.05$), unpaired t-test for right panels (****$p < 0.0001$)]. (B-C) Immunocytochemical analysis of

NR1 expression in control and ASD iN cells. Scale bar: 50 μm. (C) The expression of NR1 was significantly reduced in ASD iN cells [Control: n = 51, ASD: n = 31 (Control#1: n = 13, Control#2: n = 13, Control#3: n = 13, Control#4: n = 12, ASD#3: n = 13, ASD#4: n = 10, ASD#5: n = 8), Kruskal–Wallis test for left panel ($p < 0.0001$) followed by Dunn's multiple comparisons test (Control#1 vs. Control#3, **$p < 0.01$, Control#2 vs. ASD#3, ****$p < 0.0001$, Control#3 vs. Control#4, *$p < 0.05$, Control#3 vs. ASD#3, ****$p < 0.0001$, Control#3 vs. ASD#4, **$p < 0.01$), Mann–Whitney test for right panel (****$p < 0.0001$)].

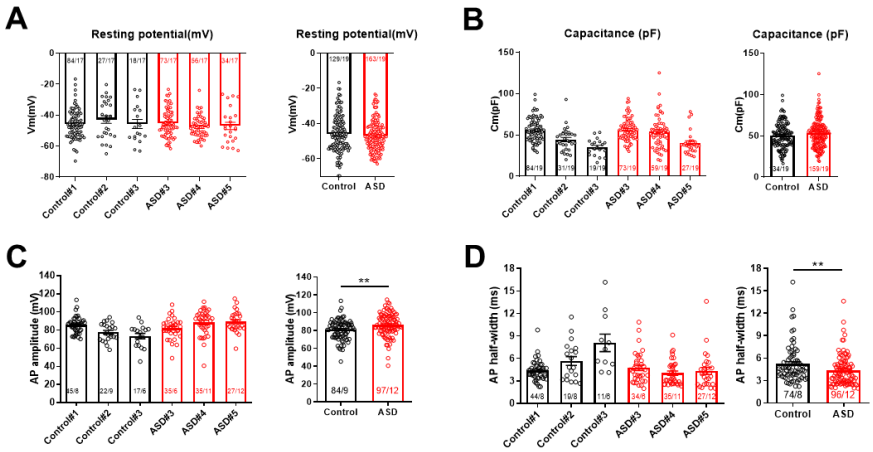

Figure 14. Basic electrophysiological properties and synaptic transmissions of iN cell lines.

(A) Resting membrane potential is unchanged in ASD iN cells as compared to control iN cells [Control: n = 129, ASD: n = 163 (Control#1: n= 84, Control#2: n= 27, Control#3: n= 18, ASD#3: n= 73, ASD#4: n= 56, ASD#5: n= 34); Mann-Whitney test, p = 0.4613]. (B) No difference in capacitance [Control: n = 134, ASD: n = 159 (Control#1: n= 84, Control#2: n= 31, Control#3: n= 19, ASD#3: n= 73, ASD#4: n= 59, ASD#5: n= 27); unpaired t-test, p = 0.1487]. (C) ASD iN cells showed an increase in AP amplitude [Control: n = 84, ASD: n = 97 (Control#1: n= 45, Control#2: n= 22, Control#3: n= 17, ASD#3: n= 35, ASD#4: n= 35, ASD#5: n= 27); unpaired t-test, p = 0.0036). (D) Significant decrease in AP half-width was detected in the ASD iN cells [Control: n = 74, ASD: n = 96 (Control#1: n= 44, Control#2: n= 19, Control#3: n= 11, ASD#3: n= 34, ASD#4: n= 35, ASD#5: n= 27); Mann-Whitney test, $^{**}p < 0.01$).

These experiments were performed in collaboration with Ja Eun Choi.

DISCUSSION

In chapter III, the transcriptomic analysis presents genetic features of downregulated genes in ASD iN cells, such as “trans-synaptic signaling”, “axon development”, and “synapse organization”. Out of various synaptic genes, NMDA-R expression is significantly reduced in the level of mRNA and protein. DSCAM is a cell adhesion molecule that contributes to the synaptic signaling to induce the grouping of post-synaptic receptors during synaptogenesis (Li, Huang et al. 2009). Both NMDA-Rs and DSCAM are located in the synaptic membrane and this proximal condition may raise the possibility to interact with each other. In this chapter, we figure out that the expression of NR1 on the neurites is decreased and NMDA-R dysfunction is observed in ASD iN cells.

DSCAM located in the post-synaptic region could be activated by FYN kinase (Groveman, Feng et al. 2012) that phosphorylates NMDA-R (Hardingham, Arnold et al. 2001, Wang, Guo et al. 2014). To sum up, reduced density of NR1 or DSCAM in ASD iN cells perhaps triggers lesser NMDA-R phosphorylation and decreased NMDA-R-mediated currents.

There are various possibilities for how *NR1* mRNA expression is decreased in ASD iN cells. Firstly, DSCAM functions as structuring

NMDA-Rs in spines (Li HL, 2009, Neuron). Cell adhesion molecules including DSCAM make connections between pre- and post-synaptic regions. Decreased expression of DSCAM perhaps inhibits synaptic signaling and reduces the demand for NMDA-Rs in spines. Secondly, the cytoplasmic domain of DSCAM can move to the nucleus to modulate other gene expressions as a transcriptional factor. Reduced DSCAM perhaps inhibits signaling to a nucleus that regulates NMDA-R transcription. The cytoplasmic domain of DSCAM interacts with nuclear import protein and changes gene expressions related to the synaptic functions (Sachse SM, 2019, EMBO J.).

CHAPTER IV

Rescue the density of NR1 and NMDA-R mediated currents through full DSCAM expression

INTRODUCTION

The previous chapter shows heterozygous DSCAM mutation results in decreased NR1 density and NMDA-R dysfunction. The next question is how DSCAM regulates NMDA-R expression and function. To answer this question, we analyze the co-localization ratio between DSCAM and NR1. For the further step, we prove whether DSCAM mutation can cause decreased NR1 expression and dysfunction of NMDA-R directly. To verify the second question, we transfect different types of exogenous DSCAM in each control and ASD iN cells.

In chapter IV, we conducted neurite analysis and proximity ligation assay (PLA) to unveil the expression of NR1 and the co-localization ratio between NR1 and DSCAM. Furthermore, we expressed full-length DSCAM and mutated DSCAM in ASD iN cells and control iN cells respectively. Then NR1 density and NMDA-R currents are observed.

EXPERIMENTAL PROCEDURES

Transfection

To evaluate the knock-down efficiency of the *hDSCAM* shRNAs, pSuper-H1-hDSCAM-shRNA-dTomato and pcDNA3-hDSCAM-FLAG constructs were co-transfected in LX293T cells using Lipofectamine 2000 or 3000 (ThermoFisher, #11668027 or #L3000008) and western blot analysis was performed using the cell lysates of the LX293T cells 2 days after the transfection.

Knock-down experiments

For knock-down experiments, pSuper-dTomato or pSuper-H1-hDSCAM shRNA-dTomato were transfected in 5–6 weeks old control iN cells and fixed with 4% paraformaldehyde 48 h after the transfection. Regarding rescue experiments, pSuper-dTomato or pSuper-H1-hDSCAM-shRNA-dTomato constructs together with pcDNA3-hDSCAM(R)-FLAG construct were co-transfected into 5–6 weeks old control iN cells (pSuper-dTomato: 2.5 ug, pSuper-H1-hDSCAM-shRNA-dTomato: 2.5 ug, pcDNA3-hDSCAM(R)-FLAG: 5 ug, Lipofectamine 2000 or 3000: 4–6 ul per well of

24-well plate) and the transfection mixture was then replaced with culture media 6 h after the transfection. After a 48-h incubation, the iN cells were fixed with 4% paraformaldehyde for immunocytochemical analysis.

Proximity ligation assay (PLA)

Generic *in situ* PLA was performed using a Duolink kit (Sigma Aldrich, DUO92101) according to the manufacturer's instructions with minor changes. Induced neuronal (iN) cells were fixed with sequential paraformaldehyde/methanol treatment and blocked with buffer (5% normal goat serum, 0.05% Triton X-100 in PBS, pH 7.4). Next, cells were incubated with primary antibodies overnight at 4℃, followed by secondary antibodies conjugated with oligonucleotides (PLA probe anti-mouse MINUS and PLA probe anti-rabbit PLUS) for 2 h at 37°C in a humidified chamber, and cells were then incubated with ligase for 30 min at 37°C. After hybridization and ligation of the DNA oligonucleotides, amplification solution along with polymerase was added. The amplified product was detected as a red signal using complementary fluorescently labeled oligonucleotides. The PLA reactions were followed by immunocytochemistry, the addition of primary antibodies (PSD-95, NeuroMab, 75-028), and fluorophore-conjugated secondary antibodies.

RESULTS

Defective NMDA-R expressions and currents are rescued by exogenous expression of full-length DSCAM

To verify causal relationship between truncated DSCAM that caused by 2051delT point mutation and dysfunction of NMDA-R currents, we monitor the alteration of NMDA-R currents after the expression of full-length DSCAM (wild type form) and N-terminal truncated form of DSCAM (mutated form) in ASD and control iN cells respectively. NMDA-R current is significantly decreased at +60mV and +40mV holding potentials, when N-terminal truncated DSCAM is expressed in control iN cells (Figure 15A). However, full-length DSCAM expressed group shows significantly reduced NMDA-R current at +60mV and +40mV holding potential in ASD iN cells (Figure 15B). These electrophysiological data show DSCAM could modulate the function of NMDA-R.

Furthermore, when N-terminal truncated DSCAM is introduced in control iN cells, NR1 protein expression in neurite is decreased while it is enhanced in response to the introduction of full-length DSCAM in ASD iN cells by using immunocytochemistry (Figure 15C, D). Additionally, we reproduce correlation between type of DSCAM and functionality of

NMDA-R through knock-down experiment (Figure 16). NR1 and DSCAM expressions in neurite are significantly reduced in control iN cells when endogenous DSCAM becomes knocked down (Figure 16 A-E). Decreased densities in response to specific DSCAM shRNA are rescued by introducing shRNA-resistant DSCAM in control iN cells that are previously knocked down endogenous DSCAM through shRNA (Figure 16 F-I). Therefore, rescue experiments indicate that normal DSCAM is crucial for normal NR1 expression and NMDA-R currents.

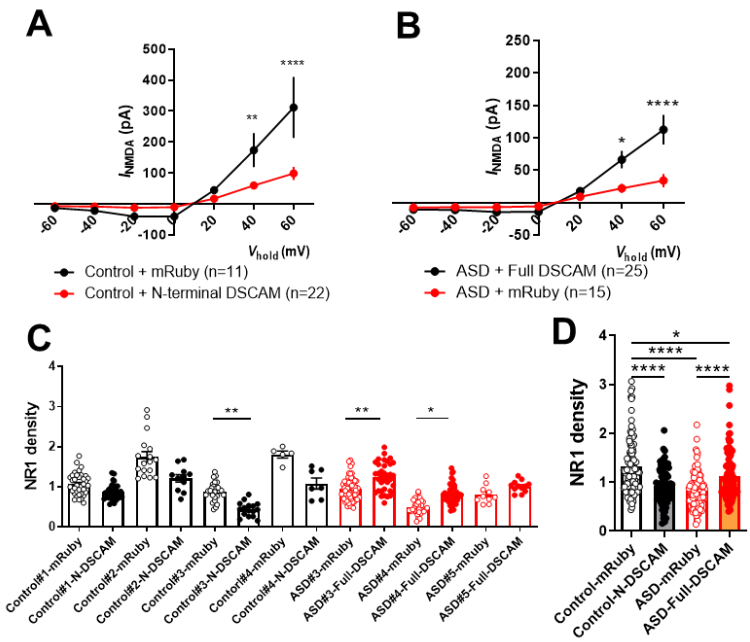

Figure 15. Exogenous DSCAM modulates NR1 density and NMDA-R currents.

(A, B) Exogenous N-terminal DSCAM expression in control iN cells led to significantly decreased INMDA at +40 and +60 mV (Control + mRuby: n = 11, Control + N-terminal DSCAM: n = 22; two-way repeated-measures ANOVA, interaction, F (6, 186) = 7.892, p < 0.0001; Bonferroni post hoc test, +40 mV, p = 0.0054; +60 mV, p < 0.0001). Exogenous overexpression of human WT DSCAM in ASD iN cells significantly increased INMDA at +40 and +60 mV (ASD + Full DSCAM: n = 25, ASD + mRuby: n = 15; two-way repeated-measures ANOVA, interaction, F (6, 228) = 6.200, p < 0.0001; Bonferroni post hoc test, +40 mV, p < 0.05; +60 mV, p < 0.0001). (C, D) Exogenous N-terminal DSCAM expression in control iN cells led to significantly decreased NR1 density (Control + mRuby: n = 86; Control#1 +

mRuby: n = 37, Control#2 + mRuby: n = 17, Control#3 + mRuby: n = 27, Control#4 + mRuby: n = 5, Control + N-terminal DSCAM: n = 65; Control#1 + N-terminal DSCAM: n = 31, Control#2 + N-terminal DSCAM: n = 11, Control#3 + N-terminal DSCAM: n = 16, Control#4 + N terminal DSCAM: n = 7) and exogenous overexpression of WT full-length DSCAM in ASD iN cells significantly increased NR1 expression (ASD + mRuby: n = 112; ASD#3 + mRuby: n = 69, ASD#4 + mRuby: n = 33, ASD#5 + mRuby: n = 10, ASD + Full-length DSCAM: n = 93; ASD#3 + Full-length DSCAM: n = 36, ASD#4 + Full-length DSCAM: n = 45, ASD#5 + Full-length DSCAM: n = 12). Kruskal–Wallis test for left panel ($p < 0.0001$) followed by Dunn's multiple comparisons test (Control#3 + mRuby vs. Control#3 + N-terminal DSCAM, $^{**}p < 0.01$, ASD#3 + mRuby vs. ASD#3 + N-terminal DSCAM, $^{*}p < 0.05$, ASD#4 + mRuby vs. ASD#4 + N-terminal DSCAM, $^{**}p < 0.01$), Kruskal–Wallis test for right panel ($p < 0.0001$) followed by Dunn's multiple comparisons test (Control + mRuby vs. Control + N-terminal DSCAM, $^{****}p < 0.0001$, Control + mRuby vs. ASD + mRuby, $^{****}p < 0.0001$, Control + mRuby vs. ASD + Full-length DSCAM, $^{*}p < 0.05$, ASD + mRuby vs. ASD + Full-length DSCAM, $^{****}p < 0.0001$).

These experiments were performed in collaboration with Ja Eun Choi and Md Ariful Islam.

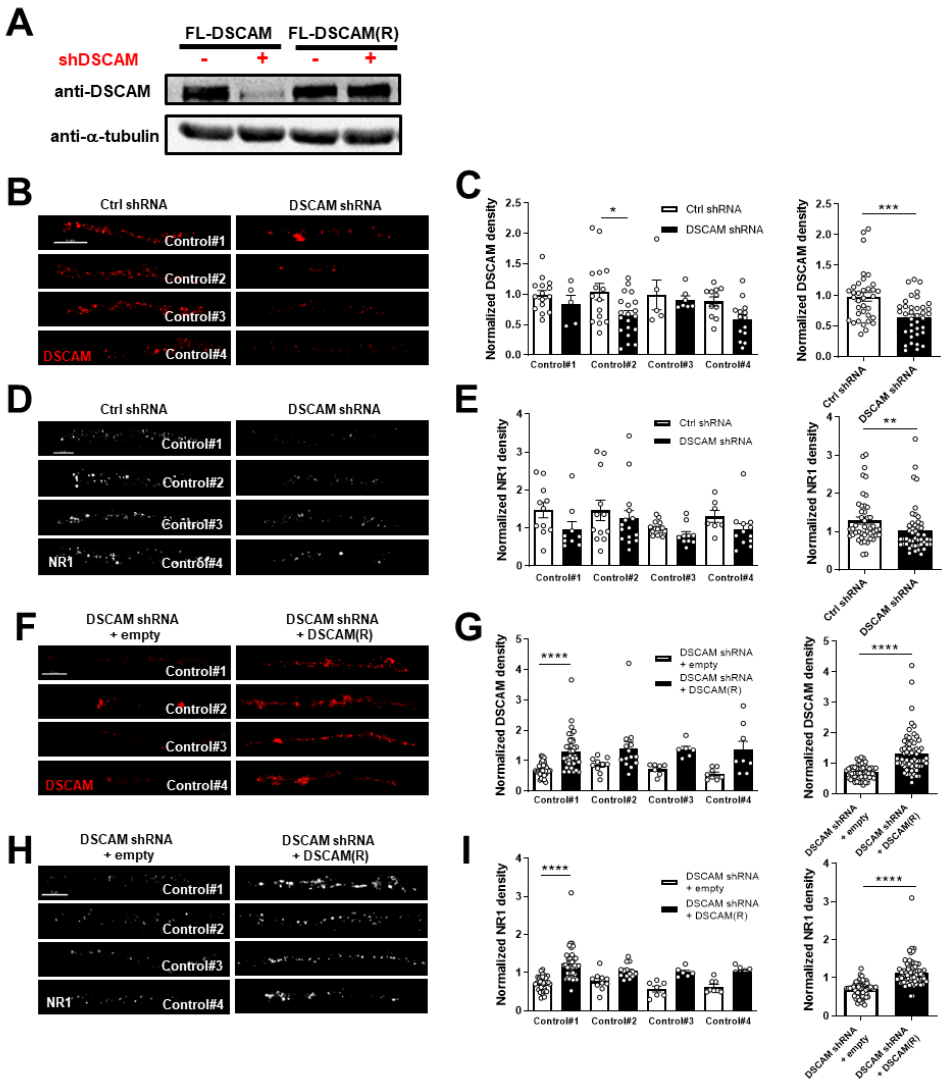

Figure 16. DSCAM density and NR1 density in iN cells during knock-down and rescue of DSCAM.

(A) Western blot analysis of the knock-down efficiency of a DSCAM shRNA. Expression of full-length DSCAM (but not of shRNA-resistant DSCAM [DSCAM(R)]) was clearly reduced using a DSCAM-specific shRNA in LX293T cells. (B-E) Knock-down of endogenous DSCAM expression using a specific DSCAM shRNA led to significantly decreased

DSCAM and NR1 density in control iN cells. Representative immunocytochemical images of DSCAM (B) and NR1 expression (D) and quantitative analysis of normalized DSCAM (C) and NR1 density (E) in control iN cells after control (Ctrl) or DSCAM shRNA expression. (DSCAM density-Ctrl shRNA: n = 46; Control#1: n = 15, Control#2: n = 15, Control#3: n = 5, Control#4: n = 11, DSCAM shRNA: n = 47; Control#1: n = 5, Control#2: n = 20, Control#3: n = 7, Control#4: n = 15, one-way ANOVA for left panel, $p < 0.01$, $F_{(7, 84)} = 3.1$, Tukey's multiple comparisons test (Control#2 + control shRNA vs Control#2 + DSCAM shRNA, *$p < 0.05$), unpaired *t*-test for right panel, ***$p < 0.001$) (NR1 density-Control shRNA: n = 46; Control#1: n = 15, Control#2: n = 15, Control#3: n = 5, Control#4: n = 11, DSCAM shRNA: n = 46; Control#1: n = 5, Control#2: n = 20, Control#3: n = 7, Control#4: n = 14, Kruskal-Wallis test for left panel, $p < 0.05$, Dunn's multiple comparisons test, ns, not significant, Mann-Whitney test for right panel, **$p < 0.01$). Scale bar: 5 um. (f-g) Exogenous expression of shRNA-resistant full-length DSCAM [DSCAM(R)] combined with a shRNA against endogenous DSCAM in control iN cells rescued DSCAM density. (Zhang, Pak et al.) Representative immunocytochemical images. Scale bar: 5 um. (G) Quantitative analysis of DSCAM expression in control iN cells after expressing DSCAM shRNA only or DSCAM shRNA combined with full-length DSCAM(R). (DSCAM shRNA + empty: n = 60; Control#1: n = 33, Control#2: n = 10, Control#3: n = 7, Control#4: n = 10, DSCAM shRNA + DSCAM(R): n =70; Control#1: n = 38, Control#2: n =

14, Control#3: n = 6, Control#4: n = 12). Kruskal-Wallis test for left panel, p <0.0001, Dunn's multiple comparisons test, Control#1 + DSCAM shRNA + empty vs Control#1 + DSCAM shRNA + DSCAM(R), ****p < 0.0001, Mann-Whitney test for right panel, ****p < 0.0001. (H-I) Exogenous expression of shRNA-resistant full-length DSCAM [DSCAM(R)] combined with a shRNA against endogenous DSCAM in control iN cells rescued NR1 density. (H) Representative immunocytochemical images. Scale bar: 5 um. (I) Quantitative analysis of NR1 expression in control iN cells after expressing *DSCAM* shRNA only or *DSCAM* shRNA combined with full-length DSCAM(R) expression. (DSCAM shRNA + empty: n = 60; Control#1: n = 33, Control#2: n = 10, Control#3: n = 7, Control#4: n = 10, DSCAM shRNA + DSCAM(R): n = 70; Control#1: n = 38, Control#2: n = 14, Control#3: n = 6, Control#4: n = 12). Kruskal-Wallis test for left panel, p <0.0001, Dunn's multiple comparisons test, Control#1 + DSCAM shRNA + empty vs Control#1 + DSCAM shRNA + DSCAM(R), ****p < 0.0001, Mann-Whitney test for right panel, ****p < 0.0001.

These experiments were performed in collaboration with Ja Eun Choi, Md Ariful Islam, Yinyi Xiong, and Chae-Seok Lim.

Co-localization of NR1 and DSCAM and pERK1/2 activity are decreased in ASD iN cells

To figure out how mutated DSCAM affects NMDA-R dysfunction, we test the co-localization of DSCAM and NR1 on the neurites in iN cells. Through immunocytochemistry, we double-stained both DSCAM and NR1 with red and iRFP fluorescence respectively. Then each punctum in neurites and soma is counted, and the co-localization ratio is about 50% in neurites (Figure 17). Co-localization ratio is significantly decreased in ASD iN cells (Figure 17). ICC data are also reproduced through proximity ligation assay (PLA). in situ PLA show red fluorescence when two molecules directly interact. Consistently, PLA puncta are significantly reduced in ASD iN cells (Figure 18), indicating that DSCAM can regulate NMDA-Rs by interacting with each other on neurites.

According to previous research, the extracellular signal-regulated kinase (ERK) pathway is modulated by the calcium influx caused by NMDA-R activation, phosphorylated ERK translocate into the nucleus and regulates the expression of genes related to the synaptic plasticity (Krapivinsky, Krapivinsky et al. 2003, Wang, Fibuch et al. 2007). We suggest ERK pathway as possible downstream mechanism after DSCAM and NMDA-R interaction. We quantify the activated form of ERK, phosphor-ERK (pERK) and expression in control and ASD iN cells through

immunocytochemistry. We observe that pERK/Ngn2 ratio is significantly decreased in ASD iN cells (Figure 19), suggesting an interaction between DSCAM and NR1 might cause ASD pathology through ERK downstream pathway.

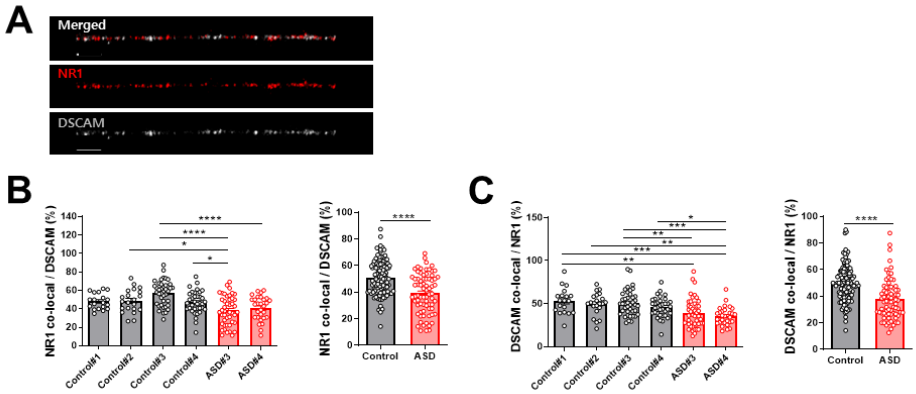

Figure 17. Decreased co-localization of DSCAM with NR1 in ASD iN cells using immunocytochemistry

(A) Immunocytochemical and processed by IMARIS program images of NR1 and DSCAM co-localization in control and ASD iN cells. Scale bar: 5 µm. (b-c) Quantitative analysis of percent co-localization of NR1 over DSCAM (Control: n = 117, ASD: n = 74 (Control#1: n = 19, Control#2: n = 21, Control#3: n = 41, Control#4: n = 36, ASD#3: n = 45, ASD#4: n = 29), one-way ANOVA for left panel (interaction, $p < 0.0001$, F(5, 185) = 10.18) followed by Bonferroni post hoc test (Control#2 vs ASD#3, *$p < 0.05$, Control#3 vs ASD#3, ****$p < 0.0001$, Control#3 vs ASD#4, ****$p < 0.0001$, Control#4 vs ASD#4, *$p < 0.05$), unpaired *t*-test for right panel, ****$p < 0.0001$) (B) or DSCAM over NR1 (Control: n = 117, ASD: n = 74 (Control#1: n = 19, Control#2: n = 21, Control#3: n = 41, Control#4: n = 36, ASD#3: n = 45, ASD#4: n = 29), one-way ANOVA for left panel (interaction, $p < 0.0001$, F(5, 185) = 7.457) followed by Bonferroni post hoc test (Control#1 vs ASD#3, **$p < 0.01$, Control#1 vs ASD#4, ***$p < 0.001$,

Control#2 vs ASD#4, $**p < 0.01$, Control#3 vs ASD#3, $**p < 0.01$, Control#3 vs ASD#4, $***p < 0.001$, Control#4 vs ASD#4, $*p < 0.05$), unpaired *t*-test for right panel, **** $p < 0.0001$) (C) in control and ASD iN cells. Note that co-localization of DSCAM and NR1 is significantly reduced in ASD iN cells as compared to control iN cells.

These experiments were performed in collaboration with Ja Eun Choi.

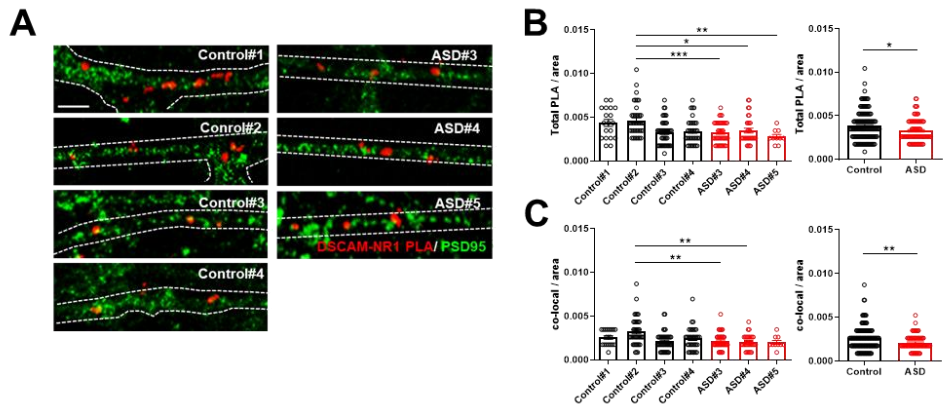

Figure 18. Decreased co-localization of DSCAM with NR1 in ASD iN cells using proximity ligation assay (PLA)

(A) Proximity ligation assay (PLA) of the co-localization between NR1 and DSCAM in iN cells. Note that the PLA signals (red puncta) were clearly observed between DSCAM and NR1. Scale bar: 100 µm. (B) Quantitative analysis of normalized total PLA signal resulted in a significant decrease in ASD iN cells [Control: n = 141, ASD: n = 85 (Control#1: n = 19, Control#2: n = 41, Control#3: n = 46, Control#4: n = 35, ASD#3: n = 44, ASD#4: n = 31, ASD#5: n = 10), one-way ANOVA for left panel (interaction, $p < 0.0001$, $F_{(6, 219)} = 5.713$) followed by Bonferroni post hoc test (Control#2 vs ASD#3, ***$p < 0.001$, Control#2 vs ASD#4, *$p < 0.05$, Control#2 vs ASD#5, **$p < 0.01$), Mann-Whitney test for right panel (*$p < 0.05$)]. Quantification of total PLA was calculated as the number of total PLA divided by image area (μm^2). (C) Co-localization between PLA signals and PSD-95 puncta also decreased in ASD iN cells [Control: n = 141, ASD: n = 85 (Control#1: n = 19, Control#2: n = 41, Control#3: n = 46, Control#4: n = 35, ASD#3: n = 44,

ASD#4: n = 31, ASD#5: n = 10), Kruskal-Wallis test for left panel ($p < 0.001$) followed by Dunn's multiple comparison test (Control#2 vs ASD#3, $^{**}p < 0.01$, Control#2 vs ASD#4, $^{**}p < 0.01$), Mann-Whitney test for right panel ($^{**}p < 0.01$)]. Quantification of co-localization of PLA signals and PSD-95 puncta was evaluated as the number of co-localized puncta divided by the image area (μm^2).

These experiments were performed in collaboration with Md Arfiul Islam.

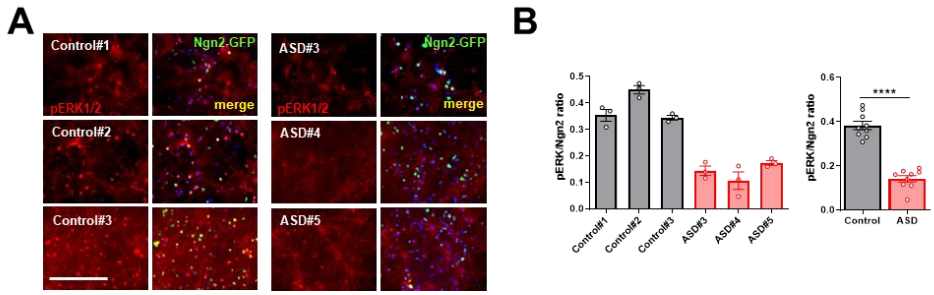

Figure 19. Reduced phosphor-ERK level in ASD iN cells

(A) Representative immunocytochemical images of phospho-ERK1/2 staining in iN cells. Scale bar: 200 µm. (B) Quantification of immunocytochemical analysis of phospho-ERK1/2 staining showed a significant decrease of phospho-ERK1/2-positive cells in ASD iN cell cultures as compared to control iN cell cultures (Control: n = 9, ASD: n = 9 from three independent cultures for each line, unpaired *t*-test for right panel, ****$p < 0.0001$).

These experiments were performed in collaboration with Md Arfiul Islam.

DISCUSSION

In the previous chapter, DSCAM mutation causes decreased NR1 expression and NMDA-R dysfunction. In this chapter, we figure out whether exogenous expression of DSCAM causes alteration of NMDA-R function and NR1 density in neurites. When N-terminal DSCAM is expressed in control iN cells, NMDA-R mediated currents and NR1 density are significantly decreased. Whereas when full-length DSCAM is expressed in ASD iN cells, currents and density are radically increased. These data show N-terminal truncated DSCAM mutation functions as the dominant-negative form. N-terminal truncated DSCAM may inhibit the active site of NMDA-R, in turn, reducing NMDA-R currents in ASD iN cells. However, exogenous full-length DSCAM restores NR1 density and NMDA-R currents. This phenomenon can be explained that overexpression of exogenous full-length DSCAM wins the dominant-negative function of endogenous truncated DSCAM. Endogenous DSCAM expression level is mimicked with DSCAM shRNA. When endogenous DSCAM expression is decreased with shRNA, NR1 density significantly decreased in control iN cells. After that, compromised NR1 expression is rescued with the reintroduction of shRNA-resistant DSCAM in control iN cells.

CHAPTER V

CONCLUSION

CONCLUSION

In this thesis, we firstly identify *de novo DSCAM* mutation in ASD patient and investigate pathological features using *in vitro* model of ASD through iPSC technique. Through RNA sequencing and qRT-PCR, we specify genes that are significantly down-regulated in ASD iN cells. Then, the expression and the functionality of the selected molecule is quantified by immunocytochemistry and patch recording. Finally, we transfect exogenous DSCAM to identify pathological features of ASD iN cells and rescue compromised traits.

In chapter II, *de novo DSCAM* mutation is found in ASD patient. *DSCAM* mutation is generated into induced neurons from iPSCs using Ngn2 differentiation method. *In vitro* disease model shows decreased DSCAM expression in the level of mRNA and protein, suggesting DSCAM mutation affects the expression of DSCAM.

In chapter III, we conducted transcriptomic analysis and figure out that genes categorized in “trans-synaptic signaling”, “axon development”, and “synaptic structure” are highly down-regulated in ASD iN cells. We specify NMDA-R components as functioning molecule among various synaptic genes that are down-regulated in ASD iN cells. mRNA level and protein density of NR1 are significantly decreased in ASD iN cells.

Consistently, NMDA-R mediated currents are also significantly decreased in ASD iN cells through patch recording. Furthermore, we unveil the expression of NR1 and co-localization ratio between NR1 and DSCAM by conducting neurite analysis and proximity ligation assay (PLA). ASD iN cells show decreased co-localization ratio compared to the control iN cells. To be specific, whether decreased co-localization ratio is caused by respectively decreased expression of DSCAM and NR1 is vague based on current PLA or neurite analysis data in the thesis. However, the fact that decreased expression of two molecules leads to silencing ERK pathway and regulating the expression of synaptic genes is obvious.

Then we figure out how this decreased interaction influences synaptic plasticity. In fact, there could be various intracellular signaling pathways related to the NMDA-R. Among them, we choose ERK pathway due to the direct connection between NMDA-R and regulation of synaptic genes. We suggest that ERK pathway could be the key node between DSCAM-NR1 interaction and altered expression of synaptic genes.

In chapter IV, we figure out how mutated DSCAM affects NMDA-R expression and function. We expressed full-length DSCAM and mutated DSCAM in ASD iN cells and control iN cells respectively. NR1 density and NMDA-R-mediated currents are decreased in control iN cells with N-terminal DSCAM, whereas increased in ASD iN cells with full-length DSCAM. These data suggest DSCAM can regulate expression and functionality of NMDA-R.

In this thesis, we firstly suggest a correlation between patient-specific *DSCAM* mutation and ASD pathology using iPSC-derived induced neurons. Furthermore, we provide ASD patient-specific research platform using iPSC technique. This research methodology may contribute to develop patient-specific treatment.

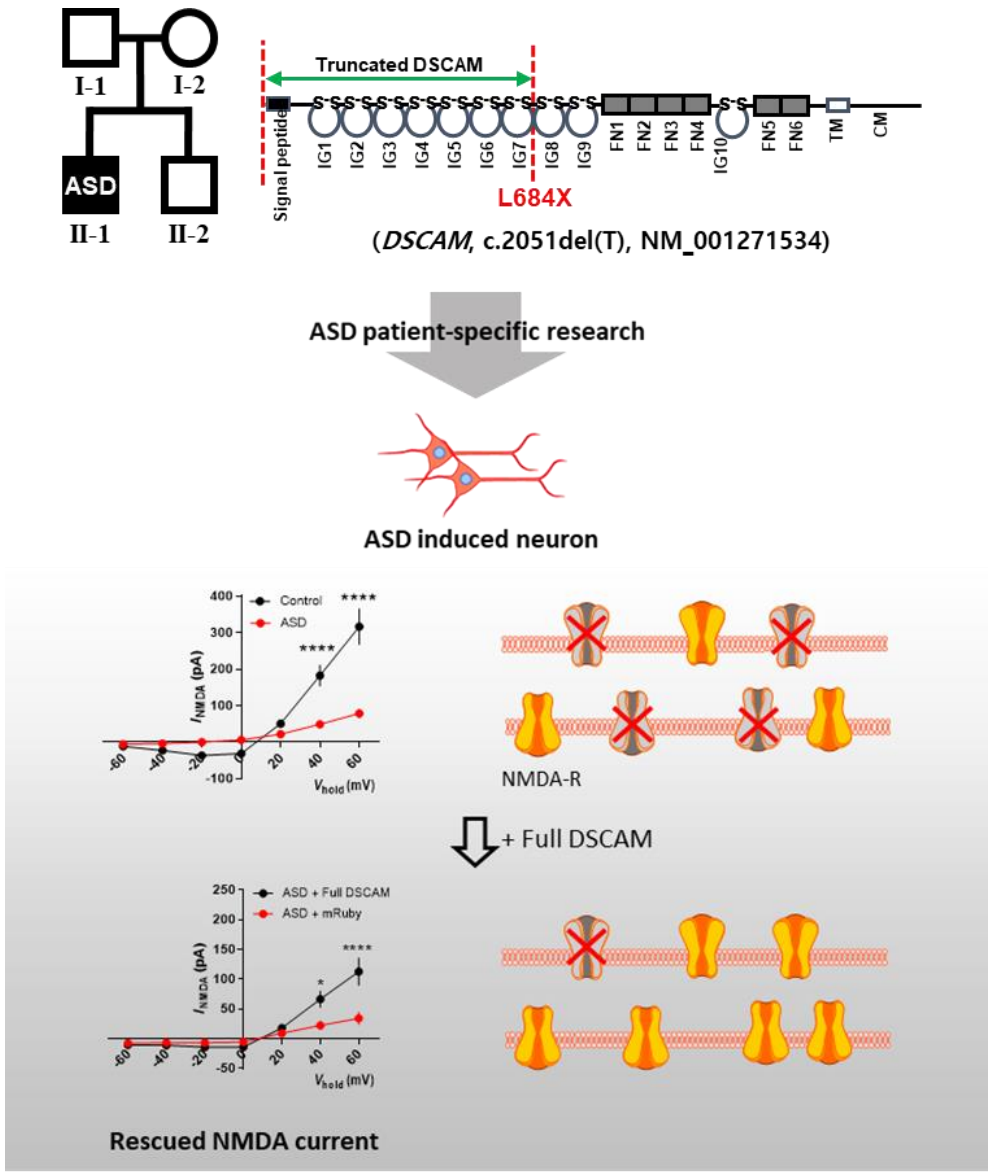

Figure 20. Graphical summary

REFERENCES

Anders, S. and W. Huber (2010). "Differential expression analysis for sequence count data." Genome Biol **11**(10): R106.

APA (2013). "Diagnostic and statistical manual of mental disorders." American Psychiatric Association **5th edition**.

C Yuen, R. K., D. Merico, M. Bookman, J. L Howe, B. Thiruvahindrapuram, R. V. Patel, J. Whitney, N. Deflaux, J. Bingham and Z. Wang (2017). "Whole genome sequencing resource identifies 18 new candidate genes for autism spectrum disorder." Nature neuroscience **20**(4): 602-611.

Chahrour, M., B. J. O'Roak, E. Santini, R. C. Samaco, R. J. Kleiman and M. C. Manzini (2016). "Current Perspectives in Autism Spectrum Disorder: From Genes to Therapy." J Neurosci **36**(45): 11402-11410.

Cotney, J., R. A. Muhle, S. J. Sanders, L. Liu, A. J. Willsey, W. Niu, W. Liu, L. Klei, J. Lei, J. Yin, S. K. Reilly, A. T. Tebbenkamp, C. Bichsel, M. Pletikos, N. Sestan, K. Roeder, M. W. State, B. Devlin and J. P. Noonan (2015). "The autism-associated chromatin modifier CHD8 regulates other autism risk genes during human neurodevelopment." Nat Commun **6**: 6404.

Cull-Candy, S. G. and D. N. Leszkiewicz (2004). "Role of distinct NMDA receptor subtypes at central synapses." Science's STKE **2004**(255): re16-re16.

De Rubeis, S., X. He, A. P. Goldberg, C. S. Poultney, K. Samocha, A.

Ercument Cicek, Y. Kou, L. Liu, M. Fromer and S. Walker (2014). "Synaptic, transcriptional and chromatin genes disrupted in autism." Nature **515**(7526): 209-215.

Dumas, T. C. (2005). "Developmental regulation of cognitive abilities: modified composition of a molecular switch turns on associative learning." Progress in neurobiology **76**(3): 189-211.

Egger, G., K. M. Roetzer, A. Noor, A. C. Lionel, H. Mahmood, T. Schwarzbraun, O. Boright, A. Mikhailov, C. R. Marshall, C. Windpassinger, E. Petek, S. W. Scherer, W. Kaschnitz and J. B. Vincent (2014). "Identification of risk genes for autism spectrum disorder through copy number variation analysis in Austrian families." Neurogenetics **15**(2): 117-127.

Fusaki, N., H. Ban, A. Nishiyama, K. Saeki and M. Hasegawa (2009). "Efficient induction of transgene-free human pluripotent stem cells using a vector based on Sendai virus, an RNA virus that does not integrate into the host genome." Proceedings of the Japan Academy, Series B **85**(8): 348-362.

Gao, R. and P. Penzes (2015). "Common mechanisms of excitatory and inhibitory imbalance in schizophrenia and autism spectrum disorders." Curr Mol Med **15**(2): 146-167.

Gilman, S. R., I. Iossifov, D. Levy, M. Ronemus, M. Wigler and D. Vitkup (2011). "Rare de novo variants associated with autism implicate a large functional network of genes involved in formation and function of synapses." Neuron **70**(5): 898-907.

Gladding, C. M. and L. A. Raymond (2011). "Mechanisms underlying NMDA receptor synaptic/extrasynaptic distribution and function." Molecular and Cellular Neuroscience **48**(4): 308-320.

Groveman, B. R., S. Feng, X. Q. Fang, M. Pflueger, S. X. Lin, E. A. Bienkiewicz and X. Yu (2012). "The regulation of N-methyl-D-aspartate receptors by Src kinase." Febs j **279**(1): 20-28.

Grzadzinski, R., M. Huerta and C. Lord (2013). "DSM-5 and autism spectrum disorders (ASDs): an opportunity for identifying ASD subtypes." Molecular Autism **4**(1): 12.

Hardingham, G. E., F. J. Arnold and H. Bading (2001). "A calcium microdomain near NMDA receptors: on switch for ERK-dependent synapse-to-nucleus communication." Nat Neurosci **4**(6): 565-566.

Hardingham, G. E. and H. Bading (2010). "Synaptic versus extrasynaptic NMDA receptor signalling: implications for neurodegenerative disorders." Nature Reviews Neuroscience **11**(10): 682-696.

Hattori, D., S. S. Millard, W. M. Wojtowicz and S. L. Zipursky (2008). "Dscam-mediated cell recognition regulates neural circuit formation." Annual review of cell and developmental biology **24**: 597-620.

He, X., S. J. Sanders, L. Liu, S. De Rubeis, E. T. Lim, J. S. Sutcliffe, G. D. Schellenberg, R. A. Gibbs, M. J. Daly, J. D. Buxbaum, M. W. State, B. Devlin and K. Roeder (2013). "Integrated model of de novo and inherited genetic variants yields greater power to identify risk genes." PLoS Genet **9**(8): e1003671.

Henson, M. A., A. C. Roberts, I. Pérez-Otaño and B. D. Philpot (2010). "Influence of the NR3A subunit on NMDA receptor functions." Progress in neurobiology **91**(1): 23-37.

Iossifov, I., B. J. O'roak, S. J. Sanders, M. Ronemus, N. Krumm, D. Levy, H. A. Stessman, K. T. Witherspoon, L. Vives and K. E. Patterson (2014). "The contribution of de novo coding mutations to autism spectrum disorder." Nature **515**(7526): 216-221.

Jia, F., K. D. Wilson, N. Sun, D. M. Gupta, M. Huang, Z. Li, N. J. Panetta, Z. Y. Chen, R. C. Robbins and M. A. Kay (2010). "A nonviral minicircle vector for deriving human iPS cells." Nature methods **7**(3): 197-199.

Jung, K. B., H. Lee, Y. S. Son, M. O. Lee, Y. D. Kim, S. J. Oh, O. Kwon, S. Cho, H. S. Cho, D. S. Kim, J. H. Oh, M. Zilbauer, J. K. Min, C. R. Jung, J. Kim and M. Y. Son (2018). "Interleukin-2 induces the in vitro maturation of human pluripotent stem cell-derived intestinal organoids." Nat Commun **9**(1): 3039.

Kenny, E. M., P. Cormican, S. Furlong, E. Heron, G. Kenny, C. Fahey, E. Kelleher, S. Ennis, D. Tropea and R. Anney (2014). "Excess of rare novel loss-of-function variants in synaptic genes in schizophrenia and autism spectrum disorders." Molecular psychiatry **19**(8): 872-879.

Kenny, E. M., P. Cormican, S. Furlong, E. Heron, G. Kenny, C. Fahey, E. Kelleher, S. Ennis, D. Tropea, R. Anney, A. P. Corvin, G. Donohoe, L. Gallagher, M. Gill and D. W. Morris (2014). "Excess of rare novel loss-of-function variants in synaptic genes in schizophrenia and autism spectrum

disorders." Mol Psychiatry **19**(8): 872-879.

Kim, D., C.-H. Kim, J.-I. Moon, Y.-G. Chung, M.-Y. Chang, B.-S. Han, S. Ko, E. Yang, K. Y. Cha and R. Lanza (2009). "Generation of human induced pluripotent stem cells by direct delivery of reprogramming proteins." Cell stem cell **4**(6): 472.

Krapivinsky, G., L. Krapivinsky, Y. Manasian, A. Ivanov, R. Tyzio, C. Pellegrino, Y. Ben-Ari, D. E. Clapham and I. Medina (2003). "The NMDA receptor is coupled to the ERK pathway by a direct interaction between NR2B and RasGRF1." Neuron **40**(4): 775-784.

Lee, E.-J., S. Y. Choi and E. Kim (2015). "NMDA receptor dysfunction in autism spectrum disorders." Current opinion in pharmacology **20**: 8-13.

Lee, Y.-K., S.-K. Hwang, S.-K. Lee, J.-E. Yang, J.-H. Kwak, H. Seo, H. Ahn, Y.-S. Lee, J. Kim, C.-S. Lim, B.-K. Kaang, J.-H. Lee, J.-A. Lee and K. Lee (2020). "Cohen Syndrome Patient iPSC-Derived Neurospheres and Forebrain-Like Glutamatergic Neurons Reveal Reduced Proliferation of Neural Progenitor Cells and Altered Expression of Synapse Genes." Journal of clinical medicine **9**(6): 1886.

Li, H., B. Handsaker, A. Wysoker, T. Fennell, J. Ruan, N. Homer, G. Marth, G. Abecasis and R. Durbin (2009). "The Sequence Alignment/Map format and SAMtools." Bioinformatics **25**(16): 2078-2079.

Li, H. L., B. S. Huang, H. Vishwasrao, N. Sutedja, W. Chen, I. Jin, R. D. Hawkins, C. H. Bailey and E. R. Kandel (2009). "Dscam mediates remodeling of glutamate receptors in Aplysia during de novo and learning-

related synapse formation." Neuron **61**(4): 527-540.

Li, J., J. Jiang, Q. Qian, Y. Xu, C. Zhang, J. Xiao, C. Du, W. Luo, G. Zou and M. Chen (2011). "Mutation of rice BC12/GDD1, which encodes a kinesin-like protein that binds to a GA biosynthesis gene promoter, leads to dwarfism with impaired cell elongation." The Plant Cell **23**(2): 628-640.

Li, S., J. M. Sukeena, A. B. Simmons, E. J. Hansen, R. E. Nuhn, I. S. Samuels and P. G. Fuerst (2015). "DSCAM promotes refinement in the mouse retina through cell death and restriction of exploring dendrites." Journal of Neuroscience **35**(14): 5640-5654.

Lord, C., T. S. Brugha, T. Charman, J. Cusack, G. Dumas, T. Frazier, E. J. Jones, R. M. Jones, A. Pickles and M. W. State (2020). "Autism spectrum disorder." Nature reviews Disease primers **6**(1): 1-23.

Maynard, K. R. and E. Stein (2012). "DSCAM contributes to dendrite arborization and spine formation in the developing cerebral cortex." Journal of Neuroscience **32**(47): 16637-16650.

McKenna, A., M. Hanna, E. Banks, A. Sivachenko, K. Cibulskis, A. Kernytsky, K. Garimella, D. Altshuler, S. Gabriel, M. Daly and M. A. DePristo (2010). "The Genome Analysis Toolkit: a MapReduce framework for analyzing next-generation DNA sequencing data." Genome Res **20**(9): 1297-1303.

Moon, I. S., S. J. Cho, I. Jin and R. Walikonis (2007). "A simple method for combined fluorescence in situ hybridization and immunocytochemistry." Mol Cells **24**(1): 76-82.

Neves, G., J. Zucker, M. Daly and A. Chess (2004). "Stochastic yet biased expression of multiple Dscam splice variants by individual cells." Nature genetics **36**(3): 240-246.

O'Roak, B. J., L. Vives, W. Fu, J. D. Egertson, I. B. Stanaway, I. G. Phelps, G. Carvill, A. Kumar, C. Lee, K. Ankenman, J. Munson, J. B. Hiatt, E. H. Turner, R. Levy, D. R. O'Day, N. Krumm, B. P. Coe, B. K. Martin, E. Borenstein, D. A. Nickerson, H. C. Mefford, D. Doherty, J. M. Akey, R. Bernier, E. E. Eichler and J. Shendure (2012). "Multiplex Targeted Sequencing Identifies Recurrently Mutated Genes in Autism Spectrum Disorders." Science **338**(6114): 1619-1622.

O'Roak, B. J., L. Vives, S. Girirajan, E. Karakoc, N. Krumm, B. P. Coe, R. Levy, A. Ko, C. Lee and J. D. Smith (2012). "Sporadic autism exomes reveal a highly interconnected protein network of de novo mutations." Nature **485**(7397): 246-250.

Okita, K., Y. Matsumura, Y. Sato, A. Okada, A. Morizane, S. Okamoto, H. Hong, M. Nakagawa, K. Tanabe and K.-i. Tezuka (2011). "A more efficient method to generate integration-free human iPS cells." Nature methods **8**(5): 409-412.

Pachernegg, S., N. Strutz-Seebohm and M. Hollmann (2012). "GluN3 subunit-containing NMDA receptors: not just one-trick ponies." Trends in neurosciences **35**(4): 240-249.

Paoletti, P., C. Bellone and Q. Zhou (2013). "NMDA receptor subunit diversity: impact on receptor properties, synaptic plasticity and disease."

Nature Reviews Neuroscience **14**(6): 383-400.

Pizzarelli, R. and E. Cherubini (2011). "Alterations of GABAergic signaling in autism spectrum disorders." Neural Plast **2011**: 297153.

Rose, S., D. M. Niyazov, D. A. Rossignol, M. Goldenthal, S. G. Kahler and R. E. Frye (2018). "Clinical and Molecular Characteristics of Mitochondrial Dysfunction in Autism Spectrum Disorder." Mol Diagn Ther **22**(5): 571-593.

Russo, F. B., A. Brito, A. M. de Freitas, A. Castanha, B. C. de Freitas and P. C. B. Beltrão-Braga (2019). "The use of iPSC technology for modeling Autism Spectrum Disorders." Neurobiology of Disease **130**: 104483.

Satterstrom, F. K., J. A. Kosmicki, J. Wang, M. S. Breen, S. De Rubeis, J. Y. An, M. Peng, R. Collins, J. Grove, L. Klei, C. Stevens, J. Reichert, M. S. Mulhern, M. Artomov, S. Gerges, B. Sheppard, X. Xu, A. Bhaduri, U. Norman, H. Brand, G. Schwartz, R. Nguyen, E. E. Guerrero, C. Dias, C. Betancur, E. H. Cook, L. Gallagher, M. Gill, J. S. Sutcliffe, A. Thurm, M. E. Zwick, A. D. Børglum, M. W. State, A. E. Cicek, M. E. Talkowski, D. J. Cutler, B. Devlin, S. J. Sanders, K. Roeder, M. J. Daly and J. D. Buxbaum (2020). "Large-Scale Exome Sequencing Study Implicates Both Developmental and Functional Changes in the Neurobiology of Autism." Cell **180**(3): 568-584.e523.

Schmucker, D., J. C. Clemens, H. Shu, C. A. Worby, J. Xiao, M. Muda, J. E. Dixon and S. L. Zipursky (2000). "Drosophila Dscam is an axon guidance receptor exhibiting extraordinary molecular diversity." Cell **101**(6): 671-684.

Searles Quick, V. B., B. Wang and M. W. State (2021). "Leveraging large

genomic datasets to illuminate the pathobiology of autism spectrum disorders." Neuropsychopharmacology **46**(1): 55-69.

Skene, N. G., J. Bryois, T. E. Bakken, G. Breen, J. J. Crowley, H. A. Gaspar, P. Giusti-Rodriguez, R. D. Hodge, J. A. Miller, A. B. Muñoz-Manchado, M. C. O'Donovan, M. J. Owen, A. F. Pardiñas, J. Ryge, J. T. R. Walters, S. Linnarsson, E. S. Lein, P. F. Sullivan and J. Hjerling-Leffler (2018). "Genetic identification of brain cell types underlying schizophrenia." Nat Genet **50**(6): 825-833.

Srivastava, A. K. and C. E. Schwartz (2014). "Intellectual disability and autism spectrum disorders: causal genes and molecular mechanisms." Neuroscience & Biobehavioral Reviews **46**: 161-174.

Tarabeux, J., O. Kebir, J. Gauthier, F. F. Hamdan, L. Xiong, A. Piton, D. Spiegelman, É. Henrion, B. Millet, F. Fathalli, R. Joober, J. L. Rapoport, L. E. DeLisi, É. Fombonne, L. Mottron, N. Forget-Dubois, M. Boivin, J. L. Michaud, P. Drapeau, R. G. Lafrenière, G. A. Rouleau, M. O. Krebs and S. D. team (2011). "Rare mutations in N-methyl-D-aspartate glutamate receptors in autism spectrum disorders and schizophrenia." Translational Psychiatry **1**(11): e55-e55.

Traynelis, S. F., L. P. Wollmuth, C. J. McBain, F. S. Menniti, K. M. Vance, K. K. Ogden, K. B. Hansen, H. Yuan, S. J. Myers and R. Dingledine (2010). "Glutamate receptor ion channels: structure, regulation, and function." Pharmacological reviews **62**(3): 405-496.

Turner, T. N., F. Hormozdiari, M. H. Duyzend, S. A. McClymont, P. W.

Hook, I. Iossifov, A. Raja, C. Baker, K. Hoekzema and H. A. Stessman (2016). "Genome sequencing of autism-affected families reveals disruption of putative noncoding regulatory DNA." The American Journal of Human Genetics **98**(1): 58-74.

Wang, J. Q., E. E. Fibuch and L. Mao (2007). "Regulation of mitogen-activated protein kinases by glutamate receptors." J Neurochem **100**(1): 1-11.

Wang, J. Q., M. L. Guo, D. Z. Jin, B. Xue, E. E. Fibuch and L. M. Mao (2014). "Roles of subunit phosphorylation in regulating glutamate receptor function." Eur J Pharmacol **728**: 183-187.

Wang, K., M. Li and H. Hakonarson (2010). "ANNOVAR: functional annotation of genetic variants from high-throughput sequencing data." Nucleic Acids Res **38**(16): e164.

Wang, T., H. Guo, B. Xiong, H. A. Stessman, H. Wu, B. P. Coe, T. N. Turner, Y. Liu, W. Zhao and K. Hoekzema (2016). "De novo genic mutations among a Chinese autism spectrum disorder cohort." Nature communications **7**(1): 1-10.

Warren, L., P. D. Manos, T. Ahfeldt, Y.-H. Loh, H. Li, F. Lau, W. Ebina, P. K. Mandal, Z. D. Smith and A. Meissner (2010). "Highly efficient reprogramming to pluripotency and directed differentiation of human cells with synthetic modified mRNA." Cell stem cell **7**(5): 618-630.

Wei, Q., X. Zhan, X. Zhong, Y. Liu, Y. Han, W. Chen and B. Li (2015). "A Bayesian framework for de novo mutation calling in parents-offspring trios." Bioinformatics **31**(9): 1375-1381.

Wen, Z., K. M. Christian, H. Song and G.-l. Ming (2016). "Modeling psychiatric disorders with patient-derived iPSCs." Current opinion in neurobiology **36**: 118-127.

Wilkins, J. and J. L. Matson (2009). "A comparison of social skills profiles in intellectually disabled adults with and without ASD." Behavior modification **33**(2): 143-155.

Wojtowicz, W. M., J. J. Flanagan, S. S. Millard, S. L. Zipursky and J. C. Clemens (2004). "Alternative splicing of Drosophila Dscam generates axon guidance receptors that exhibit isoform-specific homophilic binding." Cell **118**(5): 619-633.

Woltjen, K., I. P. Michael, P. Mohseni, R. Desai, M. Mileikovsky, R. Hämäläinen, R. Cowling, W. Wang, P. Liu and M. Gertsenstein (2009). "piggyBac transposition reprograms fibroblasts to induced pluripotent stem cells." nature **458**(7239): 766-770.

Yamakawa, K., Y.-K. Huo, M. A. Haendel, R. Hubert, X.-N. Chen, G. E. Lyons and J. R. Korenberg (1998). "DSCAM: a novel member of the immunoglobulin superfamily maps in a Down syndrome region and is involved in the development of the nervous system." Human molecular genetics **7**(2): 227-237.

Yu, J., K. Hu, K. Smuga-Otto, S. Tian, R. Stewart, I. I. Slukvin and J. A. Thomson (2009). "Human induced pluripotent stem cells free of vector and transgene sequences." Science **324**(5928): 797-801.

Zhan, X.-L., J. C. Clemens, G. Neves, D. Hattori, J. J. Flanagan, T. Hummel,

M. L. Vasconcelos, A. Chess and S. L. Zipursky (2004). "Analysis of Dscam diversity in regulating axon guidance in Drosophila mushroom bodies." Neuron **43**(5): 673-686.

Zhang, Y., C. Pak, Y. Han, H. Ahlenius, Z. Zhang, S. Chanda, S. Marro, C. Patzke, C. Acuna, J. Covy, W. Xu, N. Yang, T. Danko, L. Chen, M. Wernig and T. C. Südhof (2013). "Rapid single-step induction of functional neurons from human pluripotent stem cells." Neuron **78**(5): 785-798.

Zhou, J. and L. F. Parada (2012). "PTEN signaling in autism spectrum disorders." Curr Opin Neurobiol **22**(5): 873-879.

Zhou, W. and C. R. Freed (2009). "Adenoviral gene delivery can reprogram human fibroblasts to induced pluripotent stem cells." Stem cells **27**(11): 2667-2674.

Zhou, Y., B. Zhou, L. Pache, M. Chang, A. H. Khodabakhshi, O. Tanaseichuk, C. Benner and S. K. Chanda (2019). "Metascape provides a biologist-oriented resource for the analysis of systems-level datasets." Nat Commun **10**(1): 1523.

국문 초록

자폐 스펙트럼 장애 (ASD)는 사회적 상호작용에 어려움을 겪거나 반복적인 행동을 증상으로 하는 신경발생학적 병증이다. ASD 병증은 다양성과 복잡성으로 인해, 유전적 치료와 환자 맞춤형 연구가 어려운 실정이다. 그러나 최근 유도만능줄기세포 기술의 발전으로 환자 맞춤형 ASD 모델을 설계할 수 있는 혁신적인 방안을 제시할 수 있게 되었다. 본 논문에서 저자는 자폐아에게서 채취한 섬유아세포를 역분화시켜 유도만능줄기세포를 만들었고, 이를 재분화시켜, 자폐아가 가진 이형접합성 *DSCAM* 돌연변이를 그대로 구현한 유도 신경 (iN) 세포를 만들어냈다. ASD iN 세포는 대조 군에 비해 *DSCAM*의 mRNA와 protein이 유의미하게 감소된 상태였다. 이후, transcriptomic analysis를 통해 ASD iN 세포에 NMDA 수용체를 비롯한 시냅스 형성 및 신호 전달에 관여하는 유전자들의 발현이 감소해 있음을 발견하였다. 더불어 ASD iN 세포에서 NMDA 수용체 매개 전류 역시 급격히 감소한 것을 확인하였다. ASD iN 세포에서 감소한 NMDA 수용체 매개 전류는 정상적인 DSCAM의 발현으로 회복된 반면, 대조 군의 NMDA 수용체 매개 전류는 돌연변이 형태의 DSCAM을 발현시켰을 때, 감소한 것을 확인하였다. NMDA 수용체 구성단위 중, NR1과 DSCAM은 신경돌기에서 인접하게 위치하고 있는데, ASD iN 세포에서는 co-localization 비율이 유의미하게 감소하였다. 또한, ASD iN 세포에서 인산화 된 ERK1/2도 감소함을 보임으로써 NMDA 수용체의 기능 조절에 관여하는 가능성 있는 분자적

메커니즘을 제시하였다. 본 논문을 통해 이형접합성 *DSCAM* 돌연변이가 NMDA 수용체의 기능 저하를 통해 자폐 증상을 나타나게 함을 밝혔다.

주요어: 자폐스펙트럼 장애, DSCAM, NMDA 수용체, 유도만능줄기세포, 유도신경세포

학번: 2020-35575